R. & M. No. 2718
(10,907)
A.R.C. Technical Report

MINISTRY OF SUPPLY

AERONAUTICAL RESEARCH COUNCIL
REPORTS AND MEMORANDA

Velocity Distribution on Straight and Swept-back Wings of Small Thickness and Infinite Aspect Ratio at Zero Incidence

By

S. NEUMARK, TECHN.SC.D., A.F.R.AE.S.

LONDON: HER MAJESTY'S STATIONERY OFFICE
1952
PRICE 10*s* 6*d* NET

Velocity Distribution on Straight and Swept-back Wings of Small Thickness and Infinite Aspect Ratio at Zero Incidence

By

S. NEUMARK, TECHN.Sc.D., A.F.R.AE.S.

COMMUNICATED BY THE PRINCIPAL DIRECTOR OF SCIENTIFIC RESEARCH (AIR), MINISTRY OF SUPPLY

Reports and Memoranda No. 2713*

May, 1947

Summary.—A solution by H. Ludwieg[3], giving the velocity distribution in the central section of a thin swept-back wing of infinite aspect ratio with a biconvex profile at zero incidence, has been found erroneous. In connection with this problem, the approximate method of sources and sinks for determining velocity distribution on straight and swept-back wings is critically examined, its limitations established, and proper ways of its application to three-dimensional problems indicated. A correct solution of Ludwieg's problem is found, and generalized to give the velocity distribution over the entire wing. The method is further extended to cover a wide class of thin symmetrical wing profiles, those with rounded leading edge being, however, often intractable by this particular method.

The ultimate purpose of the investigation is to provide a reliable basis for determining the critical Mach number for swept-back wings. Further work is needed to embrace wings of finite aspect ratio and tapered wings, in particular delta-wings. The method seems adequate to deal with these more complex cases.

1. *Introduction.*—It has been widely known for some time that an increase of the critical Mach number can be obtained for a long untapered wing by setting it into an oblique position to the direction of flight. However, the simple theory of the flow past such a wing cannot be directly applied to the case of a symmetrical swept-back wing, because a considerable modification is brought about by the kink in the symmetry plane where the entire flow is essentially three-dimensional. The problem seemed to be very complex, and no attempts have been made in Britain to solve it by a direct theoretical approach. Therefore, important progress was thought to be achieved by a fairly recent German report by Ludwieg[3] who, by using a very simple and ingenious method, has given an apparently perfect solution of the problem, at least in the case of a wing with a simple biconvex profile (Fig. 4). Ludwieg rightly restricted his investigation to a thin symmetrical profile at zero incidence, for, at high speed, nearly symmetrical profiles and very small incidences only are to be reckoned with. All the difficulties of lift distribution are thus removed, and the problem can be solved by distributing suitable continuous sets of sources and sinks inside the wing in xy-plane, and by determining the maximum induced supervelocity in the central section. Ludwieg simply adapted the approximate method of sources distribution, as previously applied successfully in two-dimensional cases, to fit a swept-back wing. He found an amazingly simple and paradoxical result that, for a swept-back wing, the supervelocity distribution in the central section should be exactly similar to that of an unswept wing, merely reduced proportionally to $\cos \varphi$; in other words, that the supervelocity distribution in the central section should be identical with that at a section very distant from the symmetry plane (apart from the unessential transverse components). This does not mean, of course, that the critical Mach number should be equal for the two sections. Ludwieg applied his result to determine the critical Mach number as a function of sweep-back angle and thickness ratio, and produced charts for this purpose.

*R.A.E. Report Aero. 2200—received 6th October, 1947.

Ludwieg's work has aroused a good deal of interest in Britain and has been repeatedly quoted in publications [4,5]. A warning, therefore, must be given that his theory is fallacious, being based on an erroneous application of the method of sources and sinks in three-dimensional problems with discontinuities, such as appear in the ' knee ' of a swept-back wing. In two-dimensional cases, the distribution of induced velocities along the chord may be considered, with certain restrictions, as a limit of the corresponding distribution on the wing surface and, if the profile is thin, the former provides a sufficient approximation to the latter. However, this is not always so in three-dimensional problems, and, in Ludwieg's case, the two differ quite substantially, the difference increasing quickly with the sweep-back angle. What has been found by him is really the induced velocity distribution along the central chord *inside the wing*, and this is quite different from that at the surface.

Ludwieg himself suggested that his results, confined to the central section only, should be extended to cover the entire surface of the wing, especially its part near to the symmetry plane. This was intended to be done by the present writer, and the results are given in section 5, as developed in detail in Appendices II and III. It has been found that in the limiting case of $y \longrightarrow 0$, *i.e.*, when approaching the central section, a result different from Ludwieg's has been obtained. The velocity distribution must, however, be continuous along the entire surface, and this led to the conclusion that Ludwieg's simple result must have been wrong. Apart from this, his solution seemed improbable on purely intuitive grounds. To explain the source of error, it proved to be necessary to examine critically the whole method of sources and sinks, and this has been done in Appendices I and IV for straight and swept-back wings, respectively. The analysis resulted in determining the limitations and pecularities of the method, and led to simple formulæ giving the velocity distribution on straight wings, and in the central section of a swept-back wing, with an arbitrary profile. It appears that the method gives correct solutions for sharp-edged aerofoils, while it is likely to fail in many cases of aerofoils with rounded leading edge. For swept-back wings, the results always differ considerably from those of Ludwieg.

The entire theory has been limited in this report to the simpler case of infinite aspect ratio. However, the method can be very well extended to cover the more complex cases of finite aspect ratio and even of tapered wings, including delta-wings. There are no fundamental difficulties, and it is hoped that the algebraical complications will not prove prohibitive and that the results will be presented in future reports. It seems desirable to extend the theory in this direction before proceeding to the matter of critical Mach number. There being a strong tendency to apply wings of small aspect ratio (especially delta-wings) in high-speed design, all results pertaining to the infinite aspect ratio must be treated as a first step only, with a rather limited practical application.

Acknowledgements are due to Miss F. M. Ward who has done the computation and prepared the illustrations.

2. *Straight Wing (two-dimensional case).*—Before proceeding to study the complex case of a swept-back wing (Fig. 4), it will be useful to start by reviewing briefly two simpler cases, *viz.*: (1) the two-dimensional case of an unswept wing of infinite aspect ratio (Fig. 1) ; (2) the case of a sheared infinite wing (Fig. 2), where the velocity distribution is truly three-dimensional but can be determined by a two-dimensional method.

For a straight wing (Fig. 1), assuming its profile to be thin and symmetrical with respect to the chord, the velocity distribution may be determined approximately, to the small values of the order of thickness ratio $\vartheta = t/c$, by the method of sources and sinks distributed along the chord. The latter distribution could be determined exactly by the method of conformal transformation, should the transformation function be known for the given profile. However, even if this were the case, the formulæ for both sources- and velocity distribution would be extremely complicated for practically all types of profiles, and it would hardly be possible to extend the procedure to three-dimensional cases. That is why, in such problems, an approximate method has been more and more applied lately, based on the assumption that, at any point A of the

chord, the local source intensity q (per unit length of the chord) is proportional to the slope of the profile at its corresponding point P having the same abscissa as A. Explicitly :

$$q = -2U\frac{dz}{dx}, \qquad \ldots\ldots\ldots\ldots\ldots\ldots\ldots\ldots \quad (2.1)$$

the minus sign being due to the velocity U being directed in our figure against the x-axis. The formula may be simply explained as follows. Assuming that the velocity of the flow, both outside and inside a thin profile, differs little from U in direction and magnitude, the flux across any vertical section of the profile is given approximately by $2Uz$, its increments having to be supplied by the sources. Hence the strength qdx of an infinitesimal segment dx of the source line must be approximately equal to $2Udz$.

The resultant velocity at P may be determined by adding to $(-U)$ the velocity induced at P by the entire source-and-sink line, which may be obtained by integrating the effect of a source element $qd\bar{x}$. The integration may be simplified greatly if the induced velocity v at P (small of the order ϑ) is replaced by that at A, the error committed being generally small of a higher order. We then obtain :—

$$v_x = \int_{\text{T.E.}}^{\text{L.E.}} \frac{q(\bar{x})\,.\,d\bar{x}}{2\pi(x-\bar{x})}, \qquad \ldots\ldots\ldots\ldots\ldots\ldots\ldots \quad (2.2)$$

and, if the equation of the upper boundary of the profile is :

$$z = F(x)\,, \qquad \ldots\ldots\ldots\ldots\ldots\ldots\ldots \quad (2.3)$$

then :

$$v_x = -\frac{U}{\pi}\int_{\text{T.E.}}^{\text{L.E.}} \frac{F'(\bar{x})\,.\,d\bar{x}}{x-\bar{x}} \qquad \ldots\ldots\ldots\ldots\ldots\ldots\ldots \quad (2.4)$$

However, in this manner we introduce improper integrals, the integrand becoming infinite at $\bar{x} = x$, and the principal value is taken to represent a good approximation to the value of the velocity on the surface. This gives, of course, only the x component of the induced velocity, the z component v_z, to the order of ϑ, being simply $[-U\,.\,F'(x)]$. The latter component is unessential, however, because the resultant velocity

$$\left[(-U+v_x)^2+v_z^2\right]^{1/2}$$

equals $(-U+v_x)$ to the order of ϑ, and hence v_x alone may represent what is called super-velocity.

The entire method seems to have been found independently by several scientists in different countries, the first to introduce it in Britain having been H. B. Squire[1]. In Germany it was employed by Föttinger, Betz, Riegels[2], *etc.*, and also by Ludwieg[3]. But it seems never to have been critically examined, and its region of applicability has been rather vague*. An attempt of such a critical examination is given in Appendix I, for two-dimensional problems. It is shown that, for sharp-edged profiles, the method works well to the required degree of accuracy over 'almost the whole profile'; however, it fails in small regions near the leading and trailing edges, where it furnishes logarithmically infinite values instead of the big but finite values required for the resultant velocity becoming zero at the stagnation points (except the particular case of a true cusped edge, in which case the results are still valid at the edge). The restriction is not very stringent, as the most important thing is the maximum supervelocity which occurs far from the edges, and this can be predicted safely by the approximate method. It must be stressed, however, that the method may fail partly in the case of a profile with a rounded leading edge (*e.g.*, Fig. 20), where the maximum supervelocity occurs near to it.

*Goldstein[6], however, has indicated that the fundamental formula [(22) in Ref. 6, identical with equation (2.4) above] can be derived as a first approximation from the exact theory of Theodorsen.

The simplest case, considered by Ludwieg, and kept also as a representative example throughout the main text of this report, is that of a profile bounded by two symmetrical parabolic arcs (as shown in Fig. 1). Denoting the chord by $c = 2b$, and the thickness by t, we have :

$$z = F(x) = \frac{t}{2}\left(1 - \frac{x^2}{b^2}\right), \quad \ldots \quad (2.5)$$

$$\frac{dz}{dx} = F'(x) = -\frac{t}{b^2}\,x, \quad \ldots \quad (2.6)$$

$$q(x) = -2U \,.\, F'(x) = \frac{2Ut}{b^2}\,x, \quad \ldots \quad (2.7)$$

thus the distribution of sources and sinks is linear. Introducing in equation (2.4) and integrating from $\bar{x} = -b$ to $\bar{x} = +b$ (the principal value being taken as shown in Appendix I), we get :

$$v_x = -\frac{4Ut}{\pi c}\left(1 - \frac{x}{c}\ln\frac{b+x}{b-x}\right) = -\frac{4}{\pi}U\vartheta\left(1 - \tfrac{1}{2}\xi\ln\frac{1+\xi}{1-\xi}\right), \quad \ldots \quad (2.8)$$

$\xi = x/b$ being a non-dimensional chordwise co-ordinate varying from (-1) to $(+1)$ between the trailing and leading edge. The graph of the supervelocity over the profile is given in Fig. 1. It is naturally symmetrical and is a very good approximation, except very near to the edges where v_x tends to a logarithmic infinity, instead of the true, big but finite, values. The maximum supervelocity occurs midway, at $x = 0$, and is given by

$$\delta = \left|\frac{v_x}{U}\right|_{\max} = \frac{4}{\pi}\vartheta\,. \quad \ldots \quad (2.9)$$

This is $\sim$1·273 times more than the maximum supervelocity ratio for an elliptic profile of the same thickness ratio.

In a similar way, the approximate velocity distribution may be determined, and the maximum supervelocity found, for alternative profiles, symmetrical with respect to the chord. General formulæ and a few examples are given in Appendix I. A remarkable case is that of a thin ellipse for which the integration gives $v_x = -U\vartheta = \text{const.}$, which seems puzzling. However, the true velocity in this case may be easily found by means of conformal transformation, and it differs from this constant value by a small term of the order of ϑ^2 (except near the edges), and thus the approximate result is correct ; the maximum supervelocity being even exact. The method works well for all sharp-edged profiles, while those with rounded nose are often intractable.

3. *Sheared Wing.*—Let us now consider a flow past an infinite wing set into an oblique position to the direction of flight so that its leading and trailing edges make an angle φ with y-axis. Two cases may be examined, *viz.*: a *yawed wing* obtained by simply rotating the original wing in xy-plane through an angle φ, or a *sheared wing* obtained by shifting consecutive sections of the original wing in x direction according to linear law. In the former case the chord and profile in sections normal to the edges remain unaltered, in the latter we keep the profile unchanged in sections parallel to x-axis, *i.e.*, to the flight direction. In view of the subsequent application to the case of a kinked swept-back wing, it will be more convenient to consider a sheared wing (Fig. 2).

The velocity distribution is clearly three-dimensional now but it can be determined by resolving the flow in infinity into two components, one parallel to the wing edges (velocity $U \sin\varphi$), and the other one normal to them ($U\cos\varphi$). The velocity component along the wing at an arbitrary point P of the wing is then simply :

$$V_m = U\sin\varphi\,, \quad \ldots \quad (3.1)$$

while the normal component V_n may be determined exactly as for a two-dimensional flow past a straight wing. We have only to consider a flow with undisturbed velocity $U\cos\varphi$ past a normal

section which has also convex parabolic profile, the chord being now $c \cdot \cos\varphi$, the thickness remaining unaltered t, the chordwise co-ordinates x_c being proportionally reduced to $x_c \cos\varphi$, and the non-dimensional ξ being unaltered. The normal component is therefore, after (2.8):

$$V_n = -U\cos\varphi - \frac{4}{\pi} U\vartheta \left(1 - \tfrac{1}{2}\xi \ln\frac{1+\xi}{1-\xi}\right). \qquad (3.2)$$

Resolving along x and y-axes, we find the components V_x and V_y:

$$\left.\begin{aligned} V_x = -U + v_x &= V_n\cos\varphi - V_m\sin\varphi = -U - \frac{4}{\pi} U\vartheta\cos\varphi\left(1 - \tfrac{1}{2}\xi\ln\frac{1+\xi}{1-\xi}\right), \\ V_y = v_y &= V_n\sin\varphi + V_m\cos\varphi = -\frac{4}{\pi} U\vartheta\sin\varphi\left(1 - \tfrac{1}{2}\xi\ln\frac{1+\xi}{1-\xi}\right). \end{aligned}\right\} \qquad (3.3)$$

The maximum supervelocity in x direction (at $\xi = 0$) will then be:

$$|v_x|_{\max} = \frac{4}{\pi} U\vartheta\cos\varphi. \qquad (3.4)$$

It is particularly interesting, and important for the subsequent argument, that the same results may be obtained directly by applying the method of sources and sinks. In Fig. 1, any infinite source filament, singled out by its abscissa $\bar{x}$ and having a width $d\bar{x}$, has a strength $qd\bar{x}$. Such a filament may be thought as a system of infinitesimal point sources of strength $qd\bar{x}\,d\bar{y}$, uniformly distributed along the filament, the strength density being q per unit area. To obtain a corresponding source distribution for a sheared wing in Fig. 2, we must arrange the same source elements along lines parallel to the wing edges. We then get a system of oblique source filaments and, the total strength being unaltered, the strength per unit length in the oblique direction will be $qd\bar{x}\cos\varphi$. The total velocity induced at a point (x, y) in the xy-plane by a source filament passing through the point $(\bar{x}, 0)$ is now perpendicular to the filament and expressed by

$$\delta v = \frac{q(\bar{x}) \cdot d\bar{x} \cdot \cos\varphi}{2\pi n} = \frac{q(\bar{x}) \cdot d\bar{x}}{2\pi(x + y\tan\varphi - \bar{x})}, \qquad (3.5)$$

$q(\bar{x})$ being still given by equation (2.7). The components dv_x and dv_y are, respectively:

$$\left.\begin{aligned} dv_x = \delta v \cdot \cos\varphi &= \frac{4}{\pi} U\frac{t}{c^2}\cos\varphi\,\frac{\bar{x}\,d\bar{x}}{x + y\tan\varphi - \bar{x}}, \\ dv_y = \delta v \cdot \sin\varphi &= \frac{4}{\pi} U\frac{t}{c^2}\sin\varphi\,\frac{\bar{x}\,d\bar{x}}{x + y\tan\varphi - \bar{x}}. \end{aligned}\right\} \qquad (3.6)$$

Assuming the point (x, y) to be within the wing area (*i.e.*, $-b < x + y\tan\varphi < b$), integrating from $\bar{x} = -b$ to $\bar{x} = +b$, and taking the principal values, we get:

$$\frac{v_x}{\cos\varphi} = \frac{v_y}{\sin\varphi} = -\frac{4}{\pi} U\vartheta\left\{1 - \frac{x + y\tan\varphi}{c}\ln\frac{b + (x + y\tan\varphi)}{b - (x + y\tan\varphi)}\right\} \qquad (3.7)$$

However, in this case we have:

$$x + y\tan\varphi = b\xi, \qquad (3.8)$$

and hence:

$$\frac{v_x}{\cos\varphi} = \frac{v_y}{\sin\varphi} = -\frac{4}{\pi} U\vartheta\left(1 - \tfrac{1}{2}\xi\ln\frac{1+\xi}{1-\xi}\right), \qquad (3.9)$$

in complete agreement with equation (3.3).

This successful result suggests that a similar method may be applied for determining the velocity distribution in essentially three-dimensional cases, *e.g.*, for finite or semi-infinite sheared wings, and for finite or infinite swept-back wings—with a kink in the plane of symmetry.

4. *Swept-back Wing, Velocity Distribution in Central Section, after Ludwieg.*—In Ludwieg's report, an attempt has been made to determine the velocity distribution in the knee of a swept-back wing of infinite aspect ratio, *i.e.*, along the section in the central plane of symmetry, this section being rightly considered as particularly important (most endangered from the point of view of shock waves appearing at high speed). The calculation was based on distributing sources and sinks along kinked filaments, in an exactly similar way to that shown for a sheared wing where the filaments were straight. In this case, it is necessary to express first the velocity induced by a single kinked source-filament at any point B on the x-axis (Fig. 3). Supposing the strength of the filament to be Q volume units per second per unit length, the infinitesimal velocity induced by an element dm of the source line will be :

$$\delta v' = \frac{Q\,dm}{4\pi R^2}\,, \qquad \ldots\ldots\ldots\ldots\ldots\ldots\ldots\ldots \quad (4.1)$$

making an angle λ with x-axis ; the x component will be :

$$dv_x = \frac{Q\cos\lambda}{4\pi R^2}\,dn\,. \qquad \ldots\ldots\ldots\ldots\ldots\ldots\ldots\ldots \quad (4.2)$$

This expression may be integrated, taking into account the obvious geometric relationships :

$$R = x\frac{\cos\varphi}{\cos(\lambda+\varphi)}\,;\; m = x\frac{\sin\lambda}{\cos(\lambda+\varphi)}\,;\; dm = x\frac{\cos\varphi\,d\lambda}{\cos^2(\lambda+\varphi)}\,; \qquad \ldots \quad (4.3)$$

and we obtain :

$$v_x' = 2\int_0^\infty dv_x' = \frac{Q}{2\pi x\cos\varphi}\int_0^{\frac{\pi}{2}-\varphi}\cos\lambda\,d\lambda = \frac{Q}{2\pi x} \qquad \ldots\ldots\ldots \quad (4.4)$$

Hence, we arrive at the remarkable result that this induced velocity does not depend on sweep-back angle φ, and is the same for a straight vortex filament as for a kinked one of the same strength with an arbitrary φ. The formula obviously applies also when x is negative, and so the induced velocities at two points B and B', equidistant from origin, must be equal and opposed ; this seems paradoxical but is perfectly correct. The velocity component v_y' will obviously be 0 at the x-axis, because of symmetry.

Turning now to the complete swept-back wing (Fig. 4), we have a continuous system of infinitesimal kinked source filaments, and any one of them, singled out by the abscissa $\bar{x}$ of its vertex C, will be of strength :

$$q(\bar{x})\,.\,d\bar{x}\,.\,\cos\varphi = 2U\frac{t}{b^2}\cos\varphi\,.\,\bar{x}\,d\bar{x} \qquad \ldots\ldots\ldots\ldots \quad (4.5)$$

(*cf.* equation 2.7). This expression must be substituted for Q in (4.4), and x replaced by $(x-\bar{x})$; then we obtain the infinitesimal velocity induced at any point P of the central chord :

$$dv_x = \frac{4}{\pi}U\frac{t}{c^2}\cos\varphi\frac{\bar{x}\,d\bar{x}}{x-\bar{x}}\,, \qquad \ldots\ldots\ldots\ldots \quad (4.6)$$

whence, after integration :

$$v_x = -\frac{4}{\pi}U\vartheta\cos\varphi\left(1-\tfrac{1}{2}\xi\ln\frac{1+\xi}{1-\xi}\right). \qquad \ldots\ldots\ldots\ldots \quad (4.7)$$

It is seen that this velocity differs from that calculated for an unswept wing (2.8) only by the factor $\cos\varphi$, and is identical with the induced velocity component v_x for a sheared wing, as given by equation (3.3) or (3.9). The latter formula should hold good also for a section of a swept-back wing at an infinite distance from the x-axis. Hence Ludwieg arrives at the astonishing conclusion that the v_x distribution in the knee is the same as at infinity (and symmetrical with respect to O).

The above result has been obtained by Ludwieg and presented as plausible, without any reservations. He also used it for calculating the critical Mach number for swept-back wings. However, his solution is subject to very serious doubts. Intuitively, one feels that the v_x distribution in the knee of a swept-back wing should differ considerably from the symmetrical one of a sheared wing, the natural guess being that the maximum velocity in the knee should be higher and located further backwards. Supposing Ludwieg's solution were correct, we should obtain a very strange picture with equal values of v_x at $y = 0$ and $y \longrightarrow \infty$ on any one of the lines parallel to the edges. In such a case there should be either minima or maxima at some specified values of y. The former supposition seems quite improbable, the latter would mean that the central section would not be ' most endangered ' after all, and that the maximum supervelocity should be sought elsewhere.

The obvious first step to clear up the matter is to determine the supervelocity field over the entire wing, *i.e.*, for any values of x and y, satisfying the inequalities :

$$-b < x \pm y \tan \varphi < b, \quad .. \quad .. \quad .. \quad .. \quad .. \quad .. \quad (4.8)$$

the upper sign referring to the right-hand part of the wing. In view of the symmetry, it will suffice to consider this part only. A solution for other points in xy-plane, outside the wing area, may also be obtained but it has obviously little practical value. The most interesting will be the velocity distribution in the sections near to the x-axis (as suggested by Ludwieg himself), as in the more distant sections it must clearly tend to that of a sheared wing.

5. *Swept-back Wing, Velocity Distribution over the Entire Surface.*—We have to consider the same system of source and sink filaments as before, but we must determine the induced velocity at an arbitrary point R (x, y) of the wing area (Fig. 4). There are obviously both v_x and v_y components but v_x is of the first importance. An infinitesimal contribution to v_x due to an infinitesimal source filament will be now, as found already by Ludwieg, and as deduced in Appendix II (where also the component v_y is dealt with) :

$$dv_x = \frac{4U\vartheta \cos \varphi}{\pi c} \frac{(x - \bar{x}) - y^2 \{(x - \bar{x})^2 + y^2\}^{-1/2} \sin \varphi \sec^2 \varphi}{(x - \bar{x})^2 - y^2 \tan^2 \varphi} \bar{x}\, d\bar{x}, \quad .. \quad (5.1)$$

and it is seen that it comes to equation (4.6) for $y = 0$.

The integration of equation (5.1), and of the corresponding expression for dv_y is complicated, and particular care is needed to avoid mistakes when taking the principal value and finding the correct determination of the definite integrals. The details of the integration are given in Appendix III, and the final result (for the right hand part of the wing) is :

$$v_x = -\frac{4}{\pi} U\vartheta \cos \varphi \left(1 - \frac{x}{c} \ln E_1 - \frac{y}{c} \tan \varphi \,.\, \ln E_2\right), \quad .. \quad .. \quad .. \quad (5.2)$$

where :

$$\left.\begin{aligned} E_1 &= \frac{b + x + \sqrt{[(b + x)^2 + y^2]} \sin \varphi}{b - x - \sqrt{[(b - x)^2 + y^2]} \sin \varphi}, \\ E_2 &= \frac{b + x + y \tan \varphi}{b - x - y \tan \varphi} \cdot \frac{\sqrt{[(b - x)^2 + y^2]} + y \sec \varphi}{\sqrt{[(b + x)^2 + y^2]} + y \sec \varphi}, \end{aligned}\right\} \quad .. \quad (5.3)$$

all square roots meaning absolute values. Corresponding expressions for v_y are given in Appendix III.

It is more convenient to introduce special non-dimensional co-ordinates ξ and η in the plane xy, by putting :

$$y = b\eta \,;\, x = b\,(\xi - \eta \tan \varphi). \quad .. \quad .. \quad .. \quad .. \quad .. \quad .. \quad (5.4)$$

Half the chord b is thus taken as a basic length ; η is the non-dimensional co-ordinate *spanwise* (in y direction), varying from 0 to infinity along the right hand part of the wing ; and ξ is the non-dimensional co-ordinate *chordwise,* reckoned *from the mid-chord line* positive forwards, so that it becomes (-1) at the trailing edge, and $(+1)$ at the leading edge.

The supervelocity distribution will then be given by :

$$v_x = -\frac{4}{\pi} U\vartheta \cos\varphi \left[1 - \tfrac{1}{2}\xi \ln \frac{1+\xi+(r_1-\eta)\tan\varphi}{1-\xi-(r_2-\eta)\tan\varphi} + \tfrac{1}{2}\eta \tan\varphi \,.\, \ln \frac{r_1+(1+\xi)\sin\varphi\cos\varphi+\eta\cos 2\varphi}{r_2-(1-\xi)\sin\varphi\cos\varphi+\eta\cos 2\varphi}\right], \quad .. \quad .. \quad (5.5)$$

where :

$$r_1 = \sqrt{[(1+\xi)^2\cos^2\varphi - 2(1+\xi)\eta\sin\varphi\cos\varphi + \eta^2]},$$
$$r_2 = \sqrt{[(1-\xi)^2\cos^2\varphi + 2(1-\xi)\eta\sin\varphi\cos\varphi + \eta^2]}, \quad .. \quad .. \quad (5.6)$$

with a corresponding formula for v_y.

It is easy to verify, and it has been done in Appendix III, that when y increases indefinitely, expressions for v_x and v_y tend to (3.9) as they should do, and this is the first check of the accuracy of our results. To get a clear picture of the distribution of the induced velocities, over the entire wing, a single value of φ has been selected :

$$\varphi = 53^\circ\ 8',\ \cos\varphi = 0{\cdot}6,\ \sin\varphi = 0{\cdot}8,\ \tan\varphi = 4/3,$$

and the values of the ratios :

$$\left(-\frac{\pi}{4\vartheta\cos\varphi}\cdot\frac{v_x}{U}\right) \text{and} \left(-\frac{\pi}{4\vartheta\sin\varphi}\cdot\frac{v_y}{U}\right)$$

tabulated as functions of ξ for several chosen values of η. In Figs. 5 and 6, these values have been plotted against ξ, thus showing the distribution of induced velocity components in several sections parallel to the xz-plane. The curves marked $\eta = \infty$ relate to a distant section (or to an infinite sheared wing, according to form (3.9)); they do not differ from the supervelocity diagram in Fig. 1 for a straight wing, the factors $\cos\varphi$ and $\sin\varphi$ should be kept in mind, however.

Considering the curves of Fig. 5 marked $\eta = \infty$; 1 ; 0·5 ; 0·3 ; 0·2 ; 0·1, for sections nearer and nearer to xz plane, we notice that the maxima of v_x do increase slowly while moving gradually backwards. Similar curves in Fig. 6 show a gradual decrease of the maxima of v_y accompanied by their moving backwards first and then slowly forwards. It seems plausible that v_y tends to 0 when $\eta \longrightarrow 0$, but there are no symptoms whatsoever of v_x —curves tending back to the curve $\eta = \infty$.

6. *Limiting Case of Central Section, and Correct Velocity Distribution.*—The next step is to study the behaviour of v_x and v_y for small values of η tending to 0 ; and this has also been done in Appendix III. It appears that $v_y \longrightarrow 0$ as it should do, while the limit expression for v_x becomes :

$$\lim_{\eta\to 0} v_x = -\frac{4}{\pi} U\vartheta\cos\varphi\left[1 - \tfrac{1}{2}\xi\ln\left(\frac{1+\xi}{1-\xi}\frac{1+\sin\varphi}{1-\sin\varphi}\right)\right], \quad .. \quad .. \quad .. \quad (6.1)$$

and is *definitely different* from (4.7). The corresponding curve in Fig. 5 is marked $\eta = 0$. It is seen that this curve has the biggest maximum (in our case about 27 per cent higher than at infinity), located farthest back chordwise (in our case at $\xi_m \doteq -0{\cdot}46$, or approximately at three-quarter-chord). This result is physically not surprising, being exactly what might have been predicted intuitively—and it is claimed to be a correct solution. There is, however, an interesting mathematical feature in the fact that, while the differential (5.1) tends to that (4.6), there is no similar relationship between the integrals. This question will be dealt with in the next section, but we shall first examine our final formula (6.1) in more detail.

It is seen that at mid-chord point O($\xi = 0$) we have :

$$v_{x0} = -\frac{4}{\pi} U\vartheta\cos\varphi, \quad .. \quad .. \quad .. \quad .. \quad .. \quad .. \quad .. \quad (6.2)$$

and hence at this point only Ludwieg's result is correct ; it does not, however, represent the

maximum supervelocity. It is also seen that the difference between our formula (6.1) and that of Ludwieg (4.7) consists only in the linear term:

$$-\tfrac{1}{2}\xi \ln\frac{1+\sin\varphi}{1-\sin\varphi} = -\xi g d^{-1}\varphi \ , \qquad (6.3)$$

which represents a straight line through the origin in Fig. 5. The ordinates of this straight line must be added to those of the curve $\eta = \infty$ to give the supervelocity curve for the central section. The slope of the straight line increases with the angle of sweep-back φ, according to the march of the inverse Gudermannian function; hence the ratio of maximum supervelocity in the knee to that at infinity also increases with φ, while the position of this maximum recedes more and more backwards.

The supervelocity at mid-chord points in the central symmetry plane and at infinity being the same, there must be a point with maximum supervelocity on the median line, as shown in the diagram (Fig. 7) where several curves of supervelocity are given for a number of lines running parallel to the edges. It is clear, however, that this is not the maximum for the wing, nor even a local maximum. A few loci $v_x = \text{const.}$ (isobars) are represented approximately in Fig. 8.

7. *Explanation of Ludwieg's Error, and a General Solution for Arbitrary Profiles.*—There being no algebraic mistakes in Ludwieg's calculation, the error must lie deeper, and should be sought in the underlying principles which he has not discussed. It has been silently assumed by him that the entire approximate method of sources and sinks works correctly in all two- and three-dimensional cases; in particular, that the supervelocities calculated on the chord always agree, to the order of ϑ, with those to be found on the wing surface. Now, calculating induced velocities on the chord involves improper integrals; it is not clear a priori that such improper integrals are always equal to the limits to which the proper integrals (relating to the wing surface) tend when $z \longrightarrow 0$. It has been shown in our Appendix I that this is the case in two-dimensional problems with continuous source distribution. However, when dealing with three-dimensional problems, specially with singularities like those in the wing knee, the question must be re-examined, and this has been done in Appendix IV. It is shown there that the induced velocity component v_x in the xz plane, due to a single kinked source filament of strength Q, is expressed by:

$$v_x' = \frac{Q}{2\pi}\frac{x+\sqrt{[x^2+z^2]}\sin\varphi}{x^2+z^2+x\sqrt{[x^2+z^2]}\sin\varphi}; \qquad (7.1)$$

this is a generalization of the formula (4.4), to which it is reduced when $z = 0$. Considering the entire system of kinked source- and sink-filaments, for which Q is given by (4.5), we obtain the infinitesimal supervelocity component induced at any point (x, z) in the symmetry plane by a source filament with vertex at $\bar{x}$:

$$dv_x = \frac{4Ut\cos\varphi}{\pi c^2}\frac{x-\bar{x}+\sqrt{[(x-\bar{x})^2+z^2]}\sin\varphi}{(x-\bar{x})^2+z^2+(x-\bar{x})\sqrt{[(x-\bar{x})^2+z^2]}\sin\varphi}\bar{x}\,d\bar{x} \ . \qquad (7.2)$$

Integrating this from $\bar{x} = -b$ to $\bar{x} = +b$ (there being no improper integrals) we get:

$$-\frac{\pi v_x}{4U\vartheta\cos\varphi} = 1-\frac{x}{c}\ln\frac{\sqrt{[(b+x)^2+z^2]}+(b+x)\sin\varphi}{\sqrt{[(b-x)^2+z^2]}-(b-x)\sin\varphi}$$
$$-\frac{z}{c\cos\varphi}\left[\tan^{-1}\frac{b+x+\sqrt{[(b+x)^2+z^2]}\sin\varphi}{z\cos\varphi}\right.$$
$$\left.+\tan^{-1}\frac{\sqrt{[(b-x)^2+z^2]}\sin\varphi-(b-x)}{z\cos\varphi}\right]. \qquad (7.3)$$

Now, z tending to 0, the above expression tends to:

$$(v_z)_{z\longrightarrow 0} = -\frac{4}{\pi}U\vartheta\cos\varphi\left(1-\frac{x}{c}\ln\frac{b+x}{b-x}\frac{1+\sin\varphi}{1-\sin\varphi}\right), \qquad (7.4)$$

and this is equivalent to (6.1). The differential (7.2) tends to (4.6) when $z \longrightarrow 0$, but this does not apply to the integrals.

It is seen that we obtain the same limit values for v_x whether we approach the x-axis in xy-plane with $y \longrightarrow 0$, or in xz-plane with $z \longrightarrow 0$, and the only discordant expression is that calculated by Ludwieg for the points of the x-axis itself. It is clear that the true quantity we are trying to approximate is the v_x component at the surface of the wing. This is given by (7.3) when substituting (2.5) for z, but then we obtain values differing from (7.4) only by small quantities of the order of ϑ^2. As to Ludwieg's formula, it gives the induced velocity on the central chord *inside the wing* which differs from the true limit value. It is obvious that such discontinuities can occur because it even happens in a very simple two-dimensional case, shown in Fig. 9, where the entire system consists of one discrete source and one sink, in addition to a uniform flow. The induced velocity on the x-axis then approximates well that along the oval profile, but the approximation fails in the neighbourhood of the source and sink. At the source itself we get $v_x = \pm \infty$, while the limit of v_x when $z \longrightarrow 0$ with x constant is then finite, and very close to the value at the contour. In more complicated cases we have to deal with continuous systems of infinitesimal sources and sinks of the same kind, and similar discontinuities may again occur, appearing as differences between the improper integrals and the limits of proper integrals. We are lucky not to encounter such discrepancies in two-dimensional cases with continuous source distribution, as shown in Appendix I, and this is connected with the symmetry of the velocity field induced by a single straight source filament. In the case of a swept-back wing, however, the velocity field induced by a kinked source filament is no longer symmetrical, and the loci $v_x' = \text{const.}$ of such a field in xz-plane, according to (7.1), are shown in Fig. 10 (*cf.* Appendix IV). There is no wonder that the lucky agreement between the principal value of the improper integral and the limit value of the proper one no longer occurs, and only the latter is obviously the correct one. There might be doubts about the correctness of our general formulæ (5.2; 5.5) which involve the principal values of improper integrals. The doubts might be removed by calculating v_x at an arbitrary point (x, y, z), and then putting $z \longrightarrow 0$. However, such an intricate calculation is superfluous. The entire induced v_x may be split into two parts, one due to the portions of source filaments contained between two planes parallel to xz at the distances $(y - \varepsilon)$ and $(y + \varepsilon)$, and the other part due to the remainder of the system. The first part only involves improper integrals, and may cause errors. However, there has been no discrepancy in the case of a sheared wing (Section 3), and so there should be none for a swept-back one, *except in the plane xz*, where the present argument obviously fails; the decisive answer must then be furnished by a proper procedure of determining the limit, as done by our formulæ (7.3) and (7.4).

It may be necessary to determine supervelocities for a swept-back wing with a symmetrical section differing from the simplest parabolic one. In such cases the only change consists in replacing (2.5) by an appropriate equation of the given profile, and altering (2.7) and (4.5) accordingly. The calculation of v_x and v_y may then be performed on the same lines as in the previous special case (Section 5). For the most important *central section*, however, a simple general formula may be deduced, connecting the supervelocity in that section of a swept-back wing with that of a straight unyawed wing:

$$v_x = \left[(v_x)_{\varphi = 0} - \frac{U}{\pi} F'(x) \cdot \ln \frac{1 + \sin \varphi}{1 - \sin \varphi} \right] \cos \varphi. \quad .. \quad .. \quad .. \quad .. \qquad (7.5)$$

A proof of this formula is given in Appendix IV. Our previous result (6.1) is obviously a particular case of (7.5). A few further examples are given in Appendix IV, and illustrated by diagrams (Figs. 15 to 21). Here again, the method works well for sharp-edged profiles, but it often fails for those with rounded edges. It is clear, however, that the maximum supervelocity in the central section is always located further back, and is usually greater, than for an infinite sheared wing.*

* If the profile is not symmetrical fore-and-aft, the maximum supervelocity in the central section of a swept-back wing may be somewhat smaller than that on an infinite sheared one, for moderate values of φ.

It is seen that the approximate method of sources and sinks may be very well extended to three-dimensional problems but care is needed to avoid errors.

8. *Maximum Supervelocity over a Swept-back Wing with a Parabolic Profile.*—The supervelocity v_x in the knee of a swept-back wing with a parabolic profile can be represented, according to (6.1) or (7.4), by the formula :

$$-\frac{\pi}{4\vartheta}\cdot\frac{v_x}{U} = G(\xi, \varphi)\,.\cos\varphi, \qquad (8.1)$$

where :

$$G(\xi, \varphi) = 1 - \tfrac{1}{2}\xi\ln\frac{1+\xi}{1-\xi} - \tfrac{1}{2}\xi\ln\frac{1+\sin\varphi}{1-\sin\varphi}\,. \qquad (8.2)$$

An example of a graph of $G(\xi, \varphi)$ against ξ was given in Fig. 5 (curve marked $\eta = 0$) for one chosen value of $\varphi = 53$ deg 8 min, and the maximum ($\sim$1·27) in that case was clearly seen. Fig. 11 gives a series of such curves for φ varying from 0 to 80 deg. It is seen that corrections to Ludwieg's curve are small only if φ is small. For larger sweep-back angles they are very considerable, *e.g.*, up to 38 per cent for $\varphi = 60$ deg. The significance of this correction is best appreciated when bearing in mind that it equivalent to an equal increase of thickness ratio.

The most important, of course, is the product $G(\xi, \varphi).\cos\varphi$, and the relevant curves, for φ varying from 0 to 80 deg, have been plotted in Fig. 12. It is seen that the maximum supervelocity decreases with increasing sweep-back, but the rate of decrease is much smaller than that predicted by Ludwieg (*i.e.*, $\cos\varphi$). The broken lines in Figs. 11 and 12 show the positions and values of the maxima.

The maximum value of G, and the corresponding value ξ_m, may be found analytically. Differentiating (8.2) with respect to ξ, we get :

$$\ln\frac{1+\xi_m}{1-\xi_m} + \frac{2\xi_m}{1-\xi_m{}^2} = -\ln\frac{1+\sin\varphi}{1-\sin\varphi}\,, \qquad (8.3)$$

and substituting into (8.2) :

$$G_{\max} = \frac{1}{1-\xi_m{}^2}\,. \qquad (8.4)$$

The equation (8.3) cannot be solved explicitly for ξ_m ; for φ it gives :

$$\cos\varphi = \frac{\sqrt{\left[1-\xi_m{}^2\right]}}{\cosh\dfrac{\xi_m}{1-\xi_m{}^2} + \xi_m\sinh\dfrac{\xi_m}{1-\xi_m{}^2}} \qquad (8.5)$$

Using (8.4) and (8.5), the following table has been calculated ;

ξ_m	$\cos\varphi$	φ		$G_{\max}$	$G_{\max}\cos\varphi$
		rad	deg		
0	1	0	0·00	1	1
—0·1	0·98007	0·2000	11·46	1·0101	0·9900
—0·2	0·92108	0·4000	22·92	1·0417	0·9594
—0·3	0·82554	0·5996	34·36	1·0989	0·9071
—0·4	0·69787	0·7984	45·74	1·1905	0·8308
—0·5	0·54496	0·9945	56·98	1·3333	0·7265
—0·6	0·37715	1·1841	67·84	1·5625	0·5893
—0·7	0·21056	1·3586	77·84	1·9608	0·4127
—0·8	0·07215	1·4986	85·86	2·7778	0·2006
—0·9	0·00402	1·5668	89·77	5·2632	0·0212
—1·0	0	$\frac{\pi}{2} = 1·5708$	90·00	∞	0

The values from the table have been plotted against ξ_m in Fig. 13, and replotted against φ in Fig. 14. The curves of $G_{\max}$ show the deviation of our results from those of Ludwieg. The curve in Fig. 14 of

$$G_{\max} \cos \varphi = \frac{v_{x\ \max}}{(v_{x\ \max})_{\varphi = 0}} \qquad \ldots\ \ldots\ \ldots\ \ldots\ \ldots\ \ldots \qquad (8.6)$$

shows the true reduction of the maximum supervelocity in the knee of a swept-back wing, in comparison with that for an unswept wing. This curve should be examined in conjunction with that of $\cos \varphi$, corresponding to Ludwieg's theory. The latter gives much too optimistic a picture.

It may be noticed in the graphs that the relationship between φ and ξ_m is almost linear up to high values of φ. It is easy to show indeed that ξ_m may be developed in the following power series

$$-\xi_m = \frac{\varphi}{2} + \frac{1}{15}\left(\frac{\varphi}{2}\right)^5 + \frac{22}{315}\left(\frac{\varphi}{2}\right)^7 + \frac{232}{2835}\left(\frac{\varphi}{2}\right)^9 + \frac{15878}{15592}\left(\frac{\varphi}{2}\right)^{11} \cdots \cdots \varphi \text{ in radians} \qquad (8.7)$$

The series converges very rapidly for all values of φ, except very near to $\pi/2$, and a considerable part of the curve is approximated very well by the straight line $\xi_m = -\frac{1}{2}\varphi$.

List of Symbols

b	Half-chord of the wing profile
$c = 2b$	Chord of the wing profile
d	*See* equation (IV.8) and Fig. 10
E_1, E_2	Portmanteau symbols, *cf.* equation (5.3)
$F(x)$	Function determining the wing profile
F_1, F_2, F_3, F_4	Portmanteau symbols, *cf.* equations (III.17)
$G(\xi, \varphi)$	Function of velocity distribution in the central section of a swept wing (*cf.* equation (8.2)) with biconvex parabolic profile
$gd^{-1}\varphi$	Inverse Gudermannian function
h	Distance in Fig. 24
I_1, I_2, I_3, I_4	Integrals, *cf.* equations (III.10, 11, 12, 13)
I', I''	Integrals, *cf.* equations (IV.13, 14)
i	Index in equations (I.13, 14)
K, K_1, K''	Mean values of $F''(x)$, *cf.* equations (I.6 ; I.12 ; IV.14)
k	Parameter in equations (I.23) ff., also in equations (I.41) ff.
ln	Natural logarithm
m	Co-ordinate, parallel to the wing edges
n	Co-ordinate, normal to the wing edges
$p = \bar{x} - x$	Auxiliary variable, *cf.* equations (III.4)
Q	Intensity of a source filament, per unit length
q	Local intensity of source distribution, p.u.l
R	Distance in Fig. 3 and Fig. 22
r	Radius, *cf.* equations (I.28) ff.
r_1, r_2	Portmanteau symbols, *cf.* equations (5.6) and (III.18)
t	Thickness of the wing profile
U	Undisturbed velocity of the air flow
V	Resultant velocity
V_m	Component of the resultant velocity, parallel to the wing edges
V_n	Component of the resultant velocity, normal to the wing edges
V_x	x-component of the resultant velocity

V_y	y-component of the resultant velocity
v	Induced velocity
v_x	x-component of the induced velocity, called supervelocity
v_y	y-component of the induced velocity
v_z	z-component of the induced velocity
v_1, v_2	Components of the induced velocity in Fig. 24
x	Chordwise co-ordinate, positive forwards
$\bar{x}$	Chordwise co-ordinate of the source filament
y	Spanwise co-ordinate, positive to starboard
z	Vertical co-ordinate, positive upwards
α	Angles in Fig. 22 and 24
β	Angle in Fig. 22 and 24
γ	Angle in Fig. 22
$\delta = \lvert v_x/U \rvert_{\max}$	Maximum supervelocity ratio
ε	A small quantity
$\eta = y/b$	Non-dimensional spanwise co-ordinate on a swept or unswept wing, *cf.* equation (5.4)
θ	Angle in Fig. 1
λ	Angle in Fig. 3 and 22
μ	Fraction denoting the position of the maximum thickness, in equations (I.19) ff.
$\xi = (x + y \tan \varphi)/b$	Non-dimensional chordwise co-ordinate on a swept wing (x/b on an unswept wing), *cf.* equation (5.4)
ξ_m	Value of ξ corresponding to maximum supervelocity
ϱ	Radius-vector in Fig. 10
φ	Sweep-back angle
ψ	Angle in Fig. 10
ω	Auxiliary variable, *cf.* equation (I.37)
$\vartheta = t/c$	Thickness ratio of a wing profile

REFERENCES

No.	*Author*	*Title, etc.*
1	H. B. Squire	Review of the Calculations on Low Drag Wing Sections. A.R.C. Report 5865, Appendix II.1. April, 1942.
2	F. Riegels	Considerations on the Substitution of Profiles of Finite Thickness by Singularities of the Axis. M.A.P. Volkenrode Ref. MAP-VG89—150T. Reports and Transl. No. 150.
3	H. Ludwieg..	Improvement on the Critical Mach number of Aerofoils by Sweep-back. M.A.P. Volkenrode Ref. MAP-VG 82—84 T. Reports and Transl. No. 84.
4	R. Smelt	A Critical Review of German Research on High Speed Flow. 696th Lecture of the R.Ae.S.—*Jour. R.Ae.S.* No. 432, December, 1946, p. 915.
5	G. H. Lee	Tailless Aircraft Design Problems. Paper Presented at the Discussion of Engineering Problems of Future Aircraft, on 14th November, 1946. *Jour. R.Ae.S.* No. 434, February, 1947, pp. 121—123.
6	S. Goldstein	A Theory of Aerofoils of Small Thickness. Part I : Velocity Distributions for Symmetrical Aerofoils. A.R.C. Report 5804. June, 1942.
7	S. Neumark	Critical Mach Numbers for Swept-back Wings. *The Aeronautical Quarterly*, Vol. II, August 1950, pp. 85-110.
8	Th. v. Kármán and E. Trefftz	Potentialströmung um gegebene Tragflächenquerschnitte. *Z.F.M.*, 1918.

APPENDIX I

Approximate Method of Sources and Sinks in Two Dimensions

Let us consider a continuous distribution of sources and sinks along the chord of a symmetrical wing profile (Fig. 1). The local intensity at $\bar{P}(\bar{x})$ being $q(\bar{x})$, an infinitesimal source element of length $d\bar{x}$ will induce a velocity δv at an arbitrary point $P(x, z)$, given by:

$$\delta v = \frac{q(\bar{x}) \, . \, d\bar{x}}{2\pi r}, \qquad \text{(I.1)}$$

where $r = P\bar{P}$. The induced velocity components in x and z directions will be:

$$\left.\begin{aligned} dv_x &= \delta v \, . \, \sin\theta = \frac{q(\bar{x})}{2\pi} \frac{x - \bar{x}}{(x - \bar{x})^2 + z^2} d\bar{x} \, ; \\ dv_z &= \delta v \, . \, \cos\theta = \frac{q(\bar{x})}{2\pi} \frac{z}{(x - \bar{x})^2 + z^2} d\bar{x} \, . \end{aligned}\right\} \qquad \text{(I.2)}$$

According to the main principle of the method, as explained in Section 2, we assume:

$$q(\bar{x}) = -2U \, . \, F'(\bar{x}) \, , \qquad \text{(I.3)}$$

and then the integral components of the velocity induced at P by the entire system of sources and sinks will be:

$$v_x = -\frac{U}{\pi} \int_{-b}^{b} \frac{x - \bar{x}}{(x - \bar{x})^2 + z^2} F'(\bar{x}) \, d\bar{x} \, ; \qquad \text{(I.4)}$$

$$v_z = -\frac{U}{\pi} \int_{-b}^{b} \frac{z}{(x - \bar{x})^2 + z^2} F'(\bar{x}) \, d\bar{x} \, . \qquad \text{(I.5)}$$

We assume now that the profile is thin, so that t and $z = F(x)$ are small compared with c. Then $F'(\bar{x})$ and $F''(\bar{x})$ will be also small of the same order, except in the region of the edges if these are rounded, where both derivatives become infinite. We exclude, of course, profiles with abnormally large vertex angles at the edges, or those with abnormally large curvature locally. It is now easy to prove that, superposing the given velocity field on that of a uniform flow with velocity $(-U)$ in x direction, the profile becomes a streamline approximately, the deviations being small of second order. The formula (I.5) may be transformed as follows:

$$\begin{aligned} \frac{\pi v_z}{U} &= -F'(x) \int_{-b}^{b} \frac{z \, d\bar{x}}{(x - \bar{x})^2 + z^2} - z \int_{-b}^{b} \frac{F'(\bar{x}) - F'(x)}{(x - \bar{x})^2 + z^2} d\bar{x} \\ &= -F'(x) \, . \, \left| \tan^{-1} \frac{\bar{x} - x}{z} \right|_{\bar{x}=-b}^{+b} - z K \int_{-b}^{b} \frac{\bar{x} - x}{(\bar{x} - x)^2 + z^2} \, d\bar{x} \\ &= -F'(x) . \left(\pi - \tan^{-1} \frac{2bz}{b^2 - x^2 - z^2} \right) + \tfrac{1}{2} z K \, . \, \ln \frac{(b + x)^2 + z^2}{(b - x)^2 + z^2} , \end{aligned} \qquad \text{(I.6)}$$

where K is a certain mean value of $F''(x)$, smaller than the upper limit of $|F''(x)|$. The first definite integral obviously represents the angle LPT. We have now:

$$\lim_{z \to 0} (v_z/U) = -F'(x) \, , \qquad \text{(I.7)}$$

and at the points of the contour v_z/U differs from this limit only by small quantities of the second order, *q.e.d.*—The leading and trailing edges are exceptional points because v_z should really be 0 at these points. This means that our method distorts the shape of the profile in the neighbourhood of the edges, but the distortion is very small, consisting in the stagnation points moving

slightly forwards and backwards from L and T, respectively, and the sharp edges being replaced by small arcs. This kind of distortion does not occur if $F'(b) = 0$ or $F'(-b) = 0$, *i.e.*, when there are true cusps at either of the edges.

The entire above argument fails if either of the edges is rounded, $F'(x)$ and $F''(x)$ becoming infinite there, and there being no upper limit of $F''(x)$. In this case, every particular profile requires really a special investigation, and various singularities may occur. In most simple cases, however, the ensuing distortion of the profile is still small and does not, by itself, discredit the method.

Supposing the distortion of the profile is tolerable, the supervelocity v_x may be calculated from (I.4) which does not include improper integrals, except possibly at the edges. It may be proved, however, that the result will differ from the induced velocity at the chord:

$$(v_x)_{z=0} = -\frac{U}{\pi}\int_{-b}^{b} \frac{F'(\bar{x})}{x-\bar{x}}\,d\bar{x} \qquad \text{(I.8)}$$

only by small quantities of the second order. The integral (I.8) is an improper one, and its principal value should be taken.

To prove the assertion, we shall consider the following transformations:

$$\frac{\pi v_x}{U} = F'(x)\int_{-b}^{b} \frac{\bar{x}-x}{(\bar{x}-x)^2+z^2}d\bar{x} + \int_{-b}^{b} \frac{F'(\bar{x})-F'(x)}{(\bar{x}-x)^2+z^2}(\bar{x}-x)\,d\bar{x}$$

$$= -\tfrac{1}{2}F'(x)\,.\ln\frac{(b+x)^2+z^2}{(b-x)^2+z^2} + \int_{-b}^{b} \frac{F'(\bar{x})-F'(x)}{(\bar{x}-x)^2+z^2}(\bar{x}-x)\,d\bar{x} \qquad \text{(I.9)}$$

$$\left(\frac{\pi v_x}{U}\right)_{z=0} = F'(x)\int_{-b}^{b} \frac{d\bar{x}}{\bar{x}-x} + \int_{-b}^{b} \frac{F'(\bar{x})-F'(x)}{\bar{x}-x}\,d\bar{x}\,. \qquad \text{(I.10)}$$

In (I.10), only the first integral is improper; the principal value is found:

$$\int_{-b}^{b} \frac{d\bar{x}}{\bar{x}-x} = \int_{-b}^{x-\varepsilon} \frac{d\bar{x}}{\bar{x}-x} + \int_{x+\varepsilon}^{b} \frac{d\bar{x}}{\bar{x}-x} = \ln\frac{\varepsilon}{b+x} + \ln\frac{b-x}{\varepsilon} = \ln\frac{b-x}{b+x},$$

and hence:

$$\frac{\pi v_x}{U} = -F'(x)\,.\ln\frac{b+x}{b-x} + \int_{-b}^{b} \frac{F'(\bar{x})-F'(x)}{\bar{x}-x}\,d\bar{x} \qquad \text{(I.11)}$$

Subtracting now (I.9) from (I.11), we get:

$$\left(\frac{\pi v_x}{U}\right)_{z=0} - \frac{\pi v_x}{U} = \tfrac{1}{2}F'(x)\,.\ln\frac{1+z^2/(b+x)^2}{1+z^2/(b-x)^2} + z^2\int_{-b}^{b} \frac{F'(\bar{x})-F'(x)}{\bar{x}-x}\,\frac{d\bar{x}}{(\bar{x}-x)^2+z^2}$$

$$= \tfrac{1}{2}F'(x)\,.\ln\frac{1+z^2/(b+x)^2}{1+z^2/(b-x)^2} + zK_1\left(\pi - \tan^{-1}\frac{2bz}{b^2-x^2-z^2}\right), \qquad \text{(I.12)}$$

where K_1 is again a certain mean value of $F''(x)$, smaller than the upper limit. It is seen that the first term in (I.12) is small of the third order, the second one small of the second order.

The supervelocity v_x may now be calculated for any given profile from (I.8), or often better from (I.11) where the only improper integral has been determined once for all. It will be often convenient to expand (I.11) in a series, putting:

$$\frac{F'(\bar{x}) - F'(x)}{\bar{x} - x} = F''(x) + \frac{\bar{x} - x}{2!} F'''(x) + \frac{(\bar{x} - x)^2}{3!} F^{IV}(x) + \ldots$$

$$= \sum_{i=1}^{\infty} \frac{(\bar{x} - x)^{i-1}}{i!} F^{i+1}(x) , \qquad \ldots\ldots\ldots\ldots\ldots\ldots \quad \text{(I.13)}$$

which gives:

$$\frac{\pi v_x}{U} = - F'(x) . \ln \frac{b + x}{b - x} + \sum_{i=1}^{\infty} \frac{(-1)^{i+1} F^{i+1}(x)}{i! i} \left\{ (x + b)^i - (x - b)^i \right\}$$

$$= - F'(x) . \ln \frac{b + x}{b - x} + 2b . F''(x) - 2bx \frac{F'''(x)}{2!}$$

$$+ 2b \left(x^2 + \tfrac{1}{3} b^2\right) \frac{F^{IV}(x)}{3!} - 2b \left(x^3 + b^2 x\right) \frac{F^{V}(x)}{4!}$$

$$+ 2b \left(x^4 + 2b^2 x^2 + \tfrac{1}{5} b^4\right) \frac{F^{VI}(x)}{5!}$$

$$- 2b \left(x^5 + \tfrac{10}{3} b^2 x^3 + b^4 x\right) \frac{F^{VII}(x)}{6!} + \ldots \qquad \ldots\ldots\ldots \quad \text{(I.14)}$$

If $F(x)$ is a polynomial, the series becomes finite, and then the formula (I.14) is to be recommended to determine the velocity distribution in the most straightforward way. This is practically always the case for all sharp-edged profiles. It must be stressed that the first term in (I.14) assumes logarithmically infinite values (always positive) when x tends either to $(-b)$ or to $(+b)$. The method thus formally breaks down in small regions near the edges, where the profile gets distorted. The true value of v_x at the edges should be $(+U)$ so that they become true stagnation points. This does not mean any serious fault from the practical point of view. The theory dealing with the supervelocities assumed small of the order $\vartheta = t/c$ in comparison with U, there is no wonder that it yields infinite values where v_x equals U. The regions near the edges, where the formulæ are unreliable, are very narrow. In particular, the restriction practically never affects the calculation of the *maximum* (negative) *supervelocity* which generally occurs far from the edges.

It may be mentioned that, if $F'(b) = 0$ or $F'(-b) = 0$, one of the edges is a true cusp. In such a case the method is still valid at the respective edge, and the induced velocity at the edge is finite and small (positive).

One simple conclusion from the theory is that, for thin sharp-edged profiles, the supervelocity (in particular the maximum supervelocity) is proportional to the thickness ratio ϑ, the function $F(x)$ and all its derivatives containing this ratio as a factor.

All the above arguments again fail for profiles with one or two *rounded edges*. There being no upper limit of $F''(x)$, the mean value K_1 in (I.12) need not necessarily be small of the order ϑ. Nevertheless, the general formula (I.8) often gives quite satisfactory results, at least outside the region of the rounded edge(s). A general analysis of this case seems to be very complex and, at present, we are only able to produce a few examples. It has proved more expedient in this case to use (I.8) rather than (I.11) or (I.14), and to avoid infinite series. An interesting feature in all examples examined thus far is that the calculated induced velocity v_x remains finite (usually negative) right up to the rounded edge(s), while it becomes infinite (and positive) only at the edge itself. If the maximum negative v_x occurs far from the edge, it seems to be quite a satisfactory solution. It happens, however, especially for profiles with ' blunt ' edges (large radius

of curvature), that the calculated negative v_x increases up to the edge(s) ; then the true maximum of v_x occurs quite near to the edge and cannot be determined at all, more so as the component v_z becomes large in this region, and may affect the maximum resultant supervelocity in an unpredictable way. In such cases there is even *no reason to expect the maximum supervelocity to be proportional to* ϑ, and the entire theory breaks down.

Example I. Biconvex profile bounded by two symmetrical parabolic arcs (*Fig.* 1).

In this simplest case, the equation of the upper arc is :

$$z = F(x) = \frac{t}{2}\left(1 - \frac{x^2}{b^2}\right), \qquad \text{(I.15)}$$

and the successive derivatives :

$$F'(x) = -\frac{tx}{b^2};\ F''(x) = -\frac{t}{b^2};\ F'''(x) = 0, \text{ etc.} \qquad \text{(I.16)}$$

The half vertex angle at both edges is $\tan^{-1} 2\vartheta$. The sources and sinks distribution is linear, as shown in Fig. 1. The supervelocity distribution is obtained from (I.14) in the simple form :

$$v_x = -\frac{4Ut}{\pi c}\left(1 - \frac{x}{c}\ln\frac{b+x}{b-x}\right) = -\frac{4}{\pi}U\vartheta\left(1 - \tfrac{1}{2}\xi\ln\frac{1+\xi}{1-\xi}\right), \qquad \text{(I.17)}$$

and is represented by the graph in Fig. 1. The maximum supervelocity ratio is :

$$\delta = \left|\frac{v_x}{U}\right|_{\max} = \frac{4}{\pi}\vartheta = 1{\cdot}273\vartheta\,. \qquad \text{(I.18)}$$

Example II. Profile bounded by two arcs of cubics (*Figs.* 15 *and* 16).

Assuming that the maximum thickness is again t, and corresponds to the abscissa $x = \mu b$, the only possible cubic satisfying the obvious geometrical conditions, is given by the equation :

$$z = F(x) = \frac{t}{2}\frac{1-3\mu^2}{(1-\mu^2)^2}\left(1 - \frac{x^2}{b^2}\right)\left(1 + \frac{2\mu}{1-3\mu^2}\frac{x}{b}\right), \qquad \text{(I.19)}$$

with successive derivatives :

$$\left.\begin{aligned} F'(x) &= \frac{t}{b}\frac{1}{(1-\mu^2)^2}\left(\mu - \frac{x}{b}\right)\left(1 + 3\mu\frac{x}{b}\right); \\ F''(x) &= -\frac{t}{b^2}\frac{1}{(1-\mu^2)^2}\left(1 - 3\mu^2 + 6\mu\frac{x}{b}\right); \\ F'''(x) &= -\frac{6\mu}{(1-\mu^2)^2}\frac{t}{b^3} = \text{const.} \end{aligned}\right\} \qquad \text{(I.20)}$$

The vertex angles τ and τ' at leading edge and trailing edge are given respectively by :

$$\tan\frac{\tau}{2} = \frac{2(1+3\mu)}{(1-\mu^2)(1+\mu)}\vartheta\ ;\ \tan\frac{\tau'}{2} = \frac{2(1-3\mu)}{(1-\mu^2)(1-\mu)}\vartheta. \qquad \text{(I.21)}$$

It is seen that μ may only vary between $(+\frac{1}{3})$ and $(-\frac{1}{3})$, there being cusps at leading edge or trailing edge in the limiting cases. If $\mu = 0$, we come back to the parabolic profile of the previous example. The supervelocity in the general case is again obtained from (I.14) :

$$v_x = -\frac{4U\vartheta}{\pi(1-\mu^2)^2}\left[1 - 3\mu^2 + 3\mu\xi - \tfrac{1}{2}(\xi-\mu)(3\mu\xi+1)\ln\frac{1+\xi}{1-\xi}\right] \qquad \text{(I.22)}$$

Two particular profiles of this kind, for $\mu = \frac{1}{6}$ and $\frac{1}{3}$, thickness ratio 0·2, are shown in Figs. 15 and 16 together with sources and supervelocity distribution. It is seen that the maximum supervelocity increases with the maximum thickness moving forwards, the former being located ahead of the latter.

For $\mu = \frac{1}{3}$, the formula (I.22) still holds at the cusped trailing edge, where :

$$v_x = \frac{27}{16\pi} U\vartheta = 0{\cdot}537\, U\vartheta \,.$$

Example III. Profile bounded by two arcs of symmetrical quartics (Fig. 17).

This is another generalization of the biconvex profile of the Example I. The equation of the upper arc is :

$$z = F(x) = \frac{t}{2}\left(1 - \frac{x^2}{b^2}\right)\left(1 + k\,\frac{x^2}{b^2}\right), \qquad \text{(I.23)}$$

and hence :

$$\left.\begin{aligned} F'(x) &= -\frac{tx}{b^2}\left(1 - k + 2k\,\frac{x^2}{b^2}\right);\quad F''(x) = -\frac{t}{b^2}\left(1 - k + 6k\,\frac{x^2}{b^2}\right);\\ F'''(x) &= -\frac{12kt}{b^4}\,x; \qquad\qquad F^{IV}(x) = -\frac{12kt}{b^4} = \text{const.} \end{aligned}\right\} \qquad \text{(I.24)}$$

The half vertex angle at both edges is $\tan^{-1} 2(1 + k)\,\vartheta$.

The supervelocity, from (I.14) becomes :

$$v_x = -\frac{4}{\pi} U\vartheta \left[1 - \frac{k}{3} + 2k\xi^2 - \left(\frac{1-k}{2}\,\xi + k\xi^3\right)\ln\frac{1+\xi}{1-\xi}\right], \qquad \text{(I.25)}$$

or, expanded for small ξ :

$$v_x = -\frac{4}{\pi} U\vartheta \left[1 - \frac{k}{3} - (1 - 3k)\xi^2 - \frac{1 + 5k}{3}\,\xi^4 \ldots\right] \qquad \text{(I.26)}$$

The maximum supervelocity ratio (for $\xi = 0$) is :

$$\delta = \left|\frac{v_x}{U}\right|_{\max} = \frac{4}{\pi}\vartheta\left(1 - \frac{k}{3}\right), \qquad \text{(I.27)}$$

but this is only true if $k \leqslant \frac{1}{3}$, and then, for positive k, the maximum supervelocity is smaller than for the parabolic profile. The smallest δ is obtained for $k = \frac{1}{3}$, and it amounts to :

$$\delta_{\min} = \frac{32}{9\pi}\vartheta = 1{\cdot}132\vartheta,$$

which is still 13 per cent higher than for an ellipse.

If $\frac{1}{3} < k < 1$, the profile is still smooth and convex, with blunter edges and flatter in the centre, but the velocity distribution becomes disadvantageous, with a minimum at $\xi = 0$, and two symmetrical maxima nearer to the edges. For $k > 1$ the profile itself becomes concave in its central part.

For negative values of k, the vertex angles diminish (the profile becomes concave near the edges when $k < -0{\cdot}2$), and δ increases. In the extreme case $k = -1$, there are two cusps at both edges, and then the formula (I.25) holds for the entire profile. It is then :

$$\delta = \left|\frac{v_x}{U}\right|_{\max} = \frac{16}{3\pi}\vartheta = 1{\cdot}698\vartheta\,;\quad \left(\frac{v_x}{U}\right)_{\xi=1} = \frac{8}{3\pi}\vartheta = 0{\cdot}849\vartheta.$$

A few illustrative graphs are given in Fig. 17.

Example IV. Biconvex profile bounded by two circular arcs.

The equation of the circular arc is:

$$z = F(x) = \sqrt{[r^2 - x^2]} - r + \tfrac{1}{2}t, \qquad \text{(I.28)}$$

where: $r = \dfrac{c^2 + t^2}{4t}$,

and hence:

$$F'(x) = -\frac{x}{\sqrt{[r^2 - x^2]}}. \qquad \text{(I.29)}$$

The supervelocity can be found from (I.11), after a slightly laborious transformation, in the form:

$$\frac{\pi v_x}{U} = -4\tan^{-1}\vartheta + \frac{x}{\sqrt{[r^2 - x^2]}} \cdot \ln \frac{r^2 - bx + \sqrt{[r^2 - x^2]}\sqrt{[r^2 - b^2]}}{r^2 + bx + \sqrt{[r^2 - x^2]}\sqrt{[r^2 - b^2]}} \cdot \frac{b + x}{b - x}, \qquad \text{(I.30)}$$

and the maximum supervelocity ratio will be:

$$\delta = \left|\frac{v_x}{U}\right|_{\max} = \frac{4}{\pi}\tan^{-1}\vartheta, \qquad \text{(I.31)}$$

which differs from (I.18) only by small terms of third order in ϑ.

This case is particularly interesting because an exact velocity distribution may be determined for such a profile by means of conformal transformation (Kármán and Trefftz)[8]. The true maximum velocity is:

$$V_{\max} = \frac{U}{(1 + \vartheta^2)\left(1 - \frac{2}{\pi}\tan^{-1}\vartheta\right)^2}, \qquad \text{(I.32)}$$

and hence, expanding in power series:

$$\delta = \frac{V_{\max} - U}{U} = \frac{4}{\pi}\vartheta + \left(\frac{12}{\pi^2} - 1\right)\vartheta^2 - \ldots. \qquad \text{(I.33)}$$

which differs from (I.31) only by terms of second and higher order in ϑ.

No graphs are given for this case, as they would be hardly distinguishable from those in Fig. 1 for the parabolic section. As a matter of fact, the equation of the circular arc (I.28) differs itself from that of the parabolic arc (I.15) only by small terms of higher order in ϑ, and hence, from the point of view of the first order theory, the two profiles are equivalent.

Example V. Elliptic profile (Fig. 18).

The equation of the upper arc is:

$$z = F(x) = \frac{t}{2b}\sqrt{[b^2 - x^2]}, \qquad \text{(I.34)}$$

and the first derivative:

$$F'(x) = -\frac{t}{2b}\frac{x}{\sqrt{[b^2 - x^2]}}, \qquad \text{(I.35)}$$

the strength of the sources becoming $\pm\infty$ at the ends of the chord.

The velocity v_x is best found directly from (I.8):

$$v_x = -\frac{U\vartheta}{\pi}\int_{-b}^{b} \frac{\bar{x}\,d\bar{x}}{(\bar{x} - x)\sqrt{[b^2 - \bar{x}^2]}} \qquad \text{(I.36)}$$

by means of the substitution :

$$\bar{x} = b \sin \bar{\omega}, \quad x = b \sin \omega, \qquad \text{(I.37)}$$

which gives :

$$v_x = -\frac{U\vartheta}{\pi} \int_{-\pi/2}^{\pi/2} \frac{\sin \bar{\omega}}{\sin \bar{\omega} - \sin \omega} d\bar{\omega} = -\frac{U\vartheta}{\pi} \left[\pi + \sin \omega \int_{-\pi/2}^{\pi/2} \frac{d\bar{\omega}}{\sin \bar{\omega} - \sin \omega} \right] \qquad \text{(I.38)}$$

The principal value of the improper integral is found to be zero for any ω, except $\pm\pi/2$, and hence :

$$v_x = -U\vartheta, \qquad \text{(I.39)}$$

except at the edges where $v_x = \infty$. This result seems paradoxical, the supervelocity obtained being constant along the entire profile. However, in this case the exact velocity distribution can be determined by means of conformal transformation, the result being :

$$V = U(1 + \vartheta) \sqrt{\left[\frac{1 - \xi^2}{1 - (1 - \vartheta^2)\xi^2} \right]}, \qquad \text{(I.40)}$$

and it is seen that it differs from $U(1 + \vartheta)$ only by small terms of the order ϑ^2, except near the edges. A graph of the exact supervelocity is given in Fig. 18.

The remarkable fact is that the true maximum supervelocity is $U\vartheta$, being exactly equal to that given by (I.39). It seems to be the smallest maximum supervelocity obtainable for a profile with a given thickness ratio ϑ. The maximum supervelocity for the parabolic profile in Example I was 1·273 times larger, that in Example II—still higher. In Example III, it has been proved impossible to reduce the ratio below 1·13.

Example VI. Modified symmetrical profile with rounded edges (*Fig.* 19).

Assuming :

$$z = F(x) = \frac{t}{2b} [b^2 - x^2]^{1/2} \left(1 + k \frac{x^2}{b^2} \right), \qquad \text{(I.41)}$$

we get :

$$\left.\begin{aligned} F'(x) &= -\frac{tx}{2b^3} \frac{(1 - 2k)b^2 + 3kx^2}{[b^2 - x^2]^{1/2}}; \\ F''(x) &= -\frac{t}{2b^3} \frac{(1 - 2k)b^4 + 9kb^2 x^2 + 3kx^4}{(b^2 - x^2)^{3/2}}. \end{aligned}\right\} \qquad \text{(I.42)}$$

The profile becomes an ellipse when $k = 0$. For $0 < k < \frac{1}{2}$ we obtain convex oval curves fuller than an ellipse, for $0 > k > -0{\cdot}1$ convex oval curves with sharper edges, and for $-0{\cdot}1 > k > -1$ partly concave curves, until at $k = -1$ the edges become cusped. The supervelocity may be found as in the previous example :

$$v_x = -U\vartheta(1 - \tfrac{1}{2}k + 3k\xi^2). \qquad \text{(I.43)}$$

If k is positive then the supervelocity at $\xi = 0$ may be smaller than $U\vartheta$, but in this case it does not represent a maximum but a minimum. This is an example of blunt edges, the calculated v_x increases right up to the edges, and the true maxima cannot be found. For negative k the maximum supervelocity occurs in the middle, and it is larger than $U\vartheta$. It is clear that the maximum supervelocity must exceed $U\vartheta$ in all cases.

The case of a cusped profile ($k = -1$) is interesting. We have then :

$$F'(x) = -\frac{3tx}{b^2} \sqrt{\left[1 - \frac{x^2}{b^2} \right]}$$

and

$$v_x = -\tfrac{3}{2} U\vartheta\,(1 - 2\xi^2),$$

the supervelocity being $(-1{\cdot}5U\vartheta)$ at the summit, and $(+1{\cdot}5U\vartheta)$ at the cusped edges.

Example VII. Two simple profiles with rounded leading edge and pointed trailing edge (Figs. 20 and 21).

One such profile is given by:

$$\left.\begin{aligned} z = F(x) &= \frac{3}{16}\sqrt{6}\,.\,t\left[1 - \frac{x}{b}\right]^{1/2}\left(1 + \frac{x}{b}\right), \\ F'(x) &= \tfrac{3}{16}\sqrt{6}\,.\,\vartheta(1 - 3\xi)\,(1 - \xi)^{-1/2}, \end{aligned}\right\} \quad .. \quad .. \quad \text{(I.44)}$$

the maximum thickness being located at $\xi = \frac{1}{3}$, *i.e.*, at 33 per cent chord. The supervelocity becomes:

$$v_x = -\frac{9\sqrt{3}}{4\pi} U\vartheta\left[1 + \frac{3\xi - 1}{6\sqrt{[2(1 - \xi)]}}\ln\frac{\sqrt{2} + \sqrt{[1 - \xi]}}{\sqrt{2} - \sqrt{[1 - \xi]}}\right], \quad .. \quad .. \quad \text{(I.45)}$$

except at the leading edge where it is infinite. The graph is given in Fig. 20, and it is seen that v_x is not maximum at $\xi = \frac{1}{3}$ but it increases right up to the leading edge.—*Our method clearly fails to provide the maximum supervelocity* in this case, the rounded leading edge being too blunt.

Another profile of this kind, with a rounded but comparatively sharp nose is represented by:

$$\left.\begin{aligned} z = F(x) &= \tfrac{1}{2}t\left[1 - \frac{x}{b}\right]^{1/2}\left(1 + \frac{x}{b}\right)\left(1 - \tfrac{1}{2}\frac{x}{b}\right), \\ F'(x) &= \tfrac{1}{4}\vartheta(5\xi^2 - 7\xi)\,(1 - \xi)^{-1/2}; \end{aligned}\right\} \quad .. \quad .. \quad \text{(I.46)}$$

the maximum thickness is located at mid-chord. The formula for the supervelocity is:

$$v_x = -\frac{U\vartheta}{2\pi}\left[\left(\tfrac{16}{3} - 5\xi\right)\sqrt{2} + \frac{7\xi - 5\xi^2}{2\sqrt{(1 - \xi)}}\ln\frac{\sqrt{2} + \sqrt{(1 - \xi)}}{\sqrt{2} - \sqrt{(1 - \xi)}}\right]. \quad .. \quad \text{(I.47)}$$

The graph in Fig. 21 gives a clear maximum at about $\xi = -0{\cdot}1$, and $\delta \simeq 1{\cdot}2$. The method works well in this case.

APPENDIX II

Velocity Induced by Finite or Infinite Straight and Kinked Source Filaments of Constant Strength

In Fig. 22, AB is a finite source filament of constant strength Q per unit length. An infinitesimal velocity $\delta v'$, induced at any point P by a source element of length dm, is:

$$\delta v' = \frac{Q dm}{4\pi R^2}. \quad .. \quad .. \quad .. \quad .. \quad .. \quad .. \quad .. \quad .. \quad \text{(II.1)}$$

Taking into account the obvious relationships:

$$m = n\tan\lambda\,;\; dm = n\sec^2\lambda\,d\lambda\,;\; R = n\sec\lambda\,, \quad .. \quad .. \quad .. \quad .. \quad \text{(II.2)}$$

we get:

$$\delta v' = \frac{Q}{4\pi n}\,d\lambda\,. \quad .. \quad .. \quad .. \quad .. \quad .. \quad .. \quad .. \quad .. \quad \text{(II.3)}$$

The components of $\delta v'$ parallel to the axes m and n become :

$$\left.\begin{aligned} dv_m' &= -\,\delta v' \,.\, \sin\lambda = -\frac{Q}{4\pi n}\ \sin\lambda\, d\lambda\,, \\ dv_n' &= \delta v' \,.\, \cos\lambda = \frac{Q}{4\pi n}\cos\lambda\, d\lambda\,, \end{aligned}\right\} \quad .. \quad .. \quad .. \quad \text{(II.4)}$$

and hence, integrating from B to A :

$$\left.\begin{aligned} v_m' &= \frac{Q}{4\pi n}(\cos\alpha - \cos\beta), \\ v_n' &= \frac{Q}{4\pi n}(\sin\alpha + \sin\beta). \end{aligned}\right\} \quad .. \quad .. \quad .. \quad .. \quad .. \quad \text{(II.5)}$$

The component v_γ' of the induced velocity in an arbitrary direction, making an angle γ with the n-axis, thus becomes :

$$v_\gamma' = v_m' \sin\gamma + v_n' \cos\gamma = \frac{Q}{4\pi n}\left\{\sin(\alpha+\gamma) + \sin(\beta-\gamma)\right\} \quad .. \quad \text{(II.6)}$$

For a *semi-infinite source filament* $\alpha = \pi/2$, and then :

$$v_m' = -\frac{Q}{4\pi n}\cos\beta\,;\ v_n' = \frac{Q}{4\pi n}(1+\sin\beta)\,; \quad .. \quad .. \quad .. \quad .. \quad \text{(II.7)}$$

$$v' = \frac{Q}{4\pi n}\left\{\cos\gamma + \sin(\beta-\gamma)\right\}. \quad .. \quad .. \quad .. \quad .. \quad .. \quad \text{(II.8)}$$

Finally, for a *source filament extending to infinity both ways*, $\alpha = \beta = \pi/2$, and then :

$$v_m' = 0\,;\ v_n' = \frac{Q}{2\pi n}, \quad .. \quad .. \quad .. \quad .. \quad .. \quad .. \quad .. \quad \text{(II.9)}$$

in agreement with the familiar formula for an infinite source filament.

It is possible now to find the components of the velocity induced at an arbitrary point A in xy-plane by a *kinked source filament of constant strength Q with a sweep-back angle φ* (Fig. 23). The x-component due to the right hand part of the filament will be obtained from (II.8) by putting $n = x\cos\varphi + y\sin\varphi\,;\ \gamma = -\varphi\,;\ \sin(\beta-\gamma) = \sin(\beta+\varphi) = y/\sqrt{(x^2+y^2)}$:

$$\left|v_x'\right|_0^\infty = \frac{Q}{4\pi(x + y\tan\varphi)}\left(1 + \frac{y}{\sqrt{(x^2+y^2)}}\sec\varphi\right). \quad .. \quad .. \quad .. \quad \text{(II.10)}$$

Replacing in (II.10) φ by $(\pi - \varphi)$, we find the corresponding contribution of the left hand part of the filament :

$$\left|v_x'\right|_{-\infty}^0 = \frac{Q}{4\pi(x - y\tan\varphi)}\left(1 - \frac{y}{\sqrt{(x^2+y^2)}}\sec\varphi\right). \quad .. \quad .. \quad .. \quad \text{(II.11)}$$

Summarising (II.10) and (II.11), we get the *total x-component* :

$$v_x' = \frac{Q}{2\pi(x^2 - y^2\tan^2\varphi)}\left(x - \frac{y^2}{\sqrt{(x^2+y^2)}}\sin\varphi\sec^2\varphi\right) .. \quad .. \quad .. \quad \text{(II.12)}$$

In a similar way, the partial y-components of the induced velocity may be found, by putting $\gamma = \pi/2 - \varphi$; $\sin(\beta - \gamma) = -\cos(\beta + \varphi) = -x/\sqrt{(x^2 + y^2)}$, and then replacing φ by $(\pi - \varphi)$:

$$\left.\begin{aligned} \left|v_y'\right|_0^\infty &= \frac{Q}{4\pi(x + y\tan\varphi)}\left(\tan\varphi - \frac{x}{\sqrt{(x^2+y^2)}}\sec\varphi\right), \\ \left|v_y'\right|_{-\infty}^0 &= -\frac{Q}{4\pi\,(x - y\tan\varphi)}\left(\tan\varphi - \frac{x}{\sqrt{(x^2+y^2)}}\sec\varphi\right), \end{aligned}\right\} \quad \ldots\ \ldots \quad \text{(II.13)}$$

and hence the *total y-component* :

$$v_y' = \frac{Q\,y\tan\varphi}{2\pi\,(x^2 - y^2\tan^2\varphi)}\left(\frac{x}{\sqrt{(x^2+y^2)}}\sec\varphi - \tan\varphi\right). \quad \ldots\ \ldots \quad \text{(II.14)}$$

The above formulæ are valid in the entire xy-plane, *provided the square roots are always considered as positive.* It is easily verified that the induced velocity becomes infinite only along the source filament.

In particular, for $y = 0$, we get :

$$(v_y')_{y=0} = 0\ ;\ (v_x')_{y=0} = \frac{Q}{2\pi x}, \quad \ldots\ \ldots\ \ldots\ \ldots\ \ldots\ \ldots\ \ldots \quad \text{(II.15)}$$

in agreement with (4.4).

APPENDIX III

Details of Calculating the Velocity Distribution over a Swept-back Wing with a Parabolic Profile

Let us consider a swept-back wing of infinite span with a parabolic profile (Fig. 4). The strength of any one of the infinitesimal source filaments, the abscissa of whose vertex is again denoted by $\bar{x}$, will be, according to (4.5) :

$$Q = q\,d\bar{x}\cos\varphi = 8U\frac{\vartheta}{c}\cos\varphi\,.\,\bar{x}\,d\bar{x}\,. \quad \ldots\ \ldots\ \ldots\ \ldots\ \ldots \quad \text{(III.1)}$$

We now obtain the infinitesimal components of the velocity induced by this source filament, replacing in (II.12) and (II.14) x by $(x - \bar{x})$, and introducing (III.1). Thus we get :

$$dv_x = \frac{4U\vartheta\cos\varphi}{\pi c}\,.\,\frac{(x-\bar{x}) - y^2\{(x-\bar{x})^2 + y^2\}^{-1/2}\sin\varphi\sec^2\varphi}{(x-\bar{x})^2 - y^2\tan^2\varphi}\,\bar{x}\,d\bar{x}, \quad \text{(III.2)}$$

$$dv_y = \frac{4U\vartheta\sin\varphi}{\pi c}\,.\,\frac{y(x-\bar{x})\{(x-\bar{x})^2 + y^2\}^{-1/2}\sec\varphi - y\tan\varphi}{(x-\bar{x})^2 - y^2\tan^2\varphi}\,\bar{x}\,d\bar{x}, \quad \text{(III.3)}$$

and these expressions must be integrated from $\bar{x} = -b$ to $\bar{x} = +b$. The integration does not present any fundamental difficulties but is rather complex. It will be convenient to introduce an auxiliary variable :

$$p = \bar{x} - x, \quad \ldots\ \ldots\ \ldots\ \ldots\ \ldots\ \ldots\ \ldots \quad \text{(III.4)}$$

and integrate from $p = -(b + x)$ to $p = b - x$. It is sufficient to consider positive y only, and then the only value of p which makes both integrands become infinite is :

$$p = y\tan\varphi \quad \ldots\ \ldots\ \ldots\ \ldots\ \ldots\ \ldots\ \ldots \quad \text{(III.5)}$$

(for $p = -y\tan\varphi$ both integrands have finite values).

After a somewhat laborious transformation, the formulæ (III.2) and (III.3) can be reduced to the following form :

$$\frac{\pi c}{4U\vartheta\cos\varphi}\,.\,\frac{dv_x}{dp} = -\frac{x + y\tan\varphi}{p - y\tan\varphi} - 1 + y\tan\varphi\,\frac{p + x}{p^2 + y^2 + y\,(p^2+y^2)^{1/2}\sec\varphi}, \ldots \quad \text{(III.6)}$$

$$\frac{\pi c}{4U\vartheta \sin\varphi}\cdot\frac{dv_y}{dp}=-\frac{x+y\tan\varphi}{p-y\tan\varphi}+\frac{px+y^2\tan\varphi}{p^2+y^2+y\,(p^2+y^2)^{1/2}\sec\varphi}-\frac{y\sec\varphi}{(p^2+y^2)^{1/2}},\qquad\text{(III.7)}$$

where only the first simple terms become infinite at $p = y\tan\varphi$, and all other terms are always finite. We then get :

$$\frac{\pi c}{4U\vartheta\cos\varphi}v_x=-c-(x+y\tan\varphi)\;I_1+y\tan\varphi\,.\,I_2+x\,.\,I_3,\qquad\ldots\qquad\ldots\qquad\text{(III.8)}$$

$$\frac{\pi c}{4U\vartheta\sin\varphi}v_y=-(x+y\tan\varphi)\;I_1+xI_2+y\tan\varphi.\;I_3-y\sec\varphi.I_4,\qquad\ldots\qquad\ldots\qquad\text{(III.9)}$$

where :

$$I_1=\int_{-(b+x)}^{b-x}\frac{dp}{p-y\tan\varphi}=-\ln\frac{b+x+y\tan\varphi}{b-x-y\tan\varphi}\;\text{(the only improper integral)}\qquad\ldots\qquad\text{(III.10)}$$

$$I_2=\int_{-(b+x)}^{b-x}\frac{p\,dp}{p^2+y^2+y\,(p^2+y^2)^{1/2}\sec\varphi}=\Big|-\ln(\sqrt{[p^2+y^2]}+y\sec\varphi)\Big|_{-(b+x)}^{b-x}$$

$$=\ln\frac{\sqrt{[(b+x)^2+y^2]}+y\sec\varphi}{\sqrt{[(b-x)^2+y^2]}+y\sec\varphi};\qquad\ldots\qquad\ldots\qquad\ldots\qquad\ldots\qquad\text{(III.11)}$$

$$I_3=\int_{-(b+x)}^{b-x}\frac{y\tan\varphi}{p^2+y^2+y\,(p^2+y^2)^{1/2}\sec\varphi}=\Big|-\ln\frac{p\cos\varphi+y\sin\varphi}{p+(p^2+y^2)^{1/2}\sin\varphi}\Big|_{-(b+x)}^{b-x}$$

$$=\ln\frac{b+x-y\tan\varphi}{b-x+y\tan\varphi}\cdot\frac{b-x+[(b-x)^2+y^2]^{1/2}\sin\varphi}{b+x-[(b+x)^2+y^2]^{1/2}\sin\varphi};\qquad\ldots\qquad\ldots\qquad\text{(III.12)}$$

$$I_4=\int_{-(b+x)}^{b-x}\frac{dp}{\sqrt{[p^2+y^2]}}=\Big|-\ln[\sqrt{(p^2+y^2)}-p]\Big|_{-(b+x)}^{b-x}$$

$$=\ln\frac{\sqrt{[(b+x)^2+y^2]}+(b+x)}{\sqrt{[(b-x)^2+y^2]}-(b-x)}.\qquad\ldots\qquad\ldots\qquad\ldots\qquad\ldots\qquad\text{(III.13)}$$

It may be noticed that the formula for the improper integral (III.10) is only valid *within the right-hand part of the wing area* ($-b-y\tan\varphi<x<b+y\tan\varphi$) ; it becomes infinite at both leading and trailing edges. All remaining integrals are valid in the entire right hand part of the xy-plane and are always finite. This applies also to I_3 in which the numerator and denominator become simultaneously zero and change sign when crossing the *extended trailing edge of the left-hand part of the wing* ($x=-b+y\tan\varphi$). However, the entire fraction under the sign of logarithm always remains finite and positive.

Introducing (III.10, 11, 12, 13) into (III.8) and (III.9), rearranging and simplifying, we finally get the following formulæ for both components of the induced velocity :

$$-\frac{\pi v_x}{4U\vartheta\cos\varphi}=1-\frac{x}{c}\ln\frac{b+x+[(b+x)^2+y^2]^{1/2}\sin\varphi}{b-x-[(b-x)^2+y^2]^{1/2}\sin\varphi}$$

$$-\frac{y}{c}\tan\varphi\,.\ln\frac{b+x+y\tan\varphi}{b-x-y\tan\varphi}\cdot\frac{[(b-x)^2+y^2]^{1/2}+y\sec\varphi}{[(b+x)^2+y^2]^{1/2}+y\sec\varphi}\qquad\ldots\qquad\ldots\qquad\text{(III.14)}$$

$$\frac{v_y}{4U\vartheta \sin\varphi} = \frac{x}{c}\ln\frac{b+x+y\tan\varphi}{b-x-y\tan\varphi}\cdot\frac{\sqrt{[(b-x)^2+y^2]}+y\sec\varphi}{\sqrt{[(b+x)^2+y^2]}+y\sec\varphi}$$
$$+\frac{y}{c}\tan\varphi\,.\ln\frac{b+x+[(b+x)^2+y^2]^{1/2}\sin\varphi}{b-x-[(b-x)^2+y^2]^{1/2}\sin\varphi}$$
$$-\frac{y}{c}\sec\varphi\,.\ln\frac{\sqrt{[(b+x)^2+y^2]}+(b+x)}{\sqrt{[(b-x)^2+y^2]}-(b-x)} \quad .. \quad .. \quad .. \quad \text{(III.15)}$$

For numerical computation and discussion, it is more convenient to introduce special non-dimensional co-ordinates ξ and η, as defined in section 5 (form 5.4). The formulæ (III. 14, 15) can then be brought to the form :

$$\left.\begin{aligned} -\frac{\pi v_x}{4U\vartheta\cos\varphi} &= 1-\tfrac{1}{2}\xi\ln F_1+\tfrac{1}{2}\eta\tan\varphi\,.\ln F_2,\\ \frac{\pi v_y}{4U\vartheta\sin\varphi} &= \tfrac{1}{2}\eta\tan\varphi\,.\ln F_2+\tfrac{1}{2}\xi\ln F_3-\tfrac{1}{2}\eta\sec\varphi\ln F_4,\end{aligned}\right\} \quad .. \quad \text{(III.16)}$$

where :

$$\left.\begin{aligned} F_1 &= \frac{1+\xi+(r_1-\eta)\tan\varphi}{1-\xi-(r_2-\eta)\tan\varphi},\\ F_2 &= \frac{r_1+(1+\xi)\sin\varphi\cos\varphi+\eta\cos 2\varphi}{r_2-(1-\xi)\sin\varphi\cos\varphi+\eta\cos 2\varphi},\\ F_3 &= \frac{1+\xi}{1-\xi}\cdot\frac{r_2+\eta}{r_1+\eta},\\ F_4 &= \frac{r_1+(1+\xi)\cos\varphi-\eta\sin\varphi}{r_2-(1-\xi)\cos\varphi-\eta\sin\varphi},\end{aligned}\right\} \quad .. \quad .. \quad .. \quad \text{(III.17)}$$

and :

$$\left.\begin{aligned} r_1 &= \sqrt{[(1+\xi)^2\cos^2\varphi-2(1+\xi)\eta\sin\varphi\cos\varphi+\eta^2]},\\ r_2 &= \sqrt{[(1-\xi)^2\cos^2\varphi+2(1-\xi)\eta\sin\varphi\cos\varphi+\eta^2]}.\end{aligned}\right\} \quad .. \quad \text{(III.18)}$$

The first check of our results may be obtained by letting η tend to infinity, whereupon the formulae should reduce to those applying for a sheared wing. Developing for large η we get :

$$\left.\begin{aligned} r_1 &= \eta-(1+\xi)\sin\varphi\cos\varphi+\frac{(1+\xi)^2}{2\eta}\cos^4\varphi\\ &\quad+\frac{(1+\xi)^3}{2\eta^2}\cos\varphi^5\sin\varphi\ldots\\ r_2 &= \eta+(1-\xi)\sin\varphi\cos\varphi+\frac{(1-\xi)^2}{2\eta}\cos^4\varphi\\ &\quad-\frac{(1-\xi)^3}{2\eta^2}\cos\varphi^5\sin\varphi\ldots\end{aligned}\right\} \quad .. \quad .. \quad \text{(III.19)}$$

$$\left.\begin{aligned} \ln F_1 &= \ln\frac{1+\xi}{1-\xi}+\frac{\sin\varphi\cos\varphi}{\eta}+\frac{3\xi}{2\eta^2}\sin^2\varphi\cos^2\varphi\ldots\\ \ln F_2 &= \frac{\xi}{\eta^2}\cos^2\varphi+\frac{1+3\xi^2}{2\eta^3}\cos^3\varphi\sin\varphi\ldots\\ \ln F_3 &= \ln\frac{1+\xi}{1-\xi}+\frac{1}{\eta}\sin\varphi\cos\varphi-\frac{\xi}{2\eta^2}\cos^2\varphi(2-3\sin^2\varphi)\ldots\\ \ln F_4 &= \frac{2}{\eta}\cos\varphi+\frac{2\xi}{\eta^2}\sin\varphi\cos^2\varphi+\frac{1+3\xi^2}{\eta^3}\cos^3\varphi(\tfrac{2}{3}-\cos^2\varphi)\quad\ldots\end{aligned}\right\} \quad \text{(III.20)}$$

and finally :

$$\left.\begin{aligned} v_x &= -\frac{4U\vartheta}{\pi}\cos\varphi\left(1-\tfrac{1}{2}\xi\ln\frac{1+\xi}{1-\xi}+\frac{\sin^2\varphi\cos^2\varphi}{4\eta^2}\ \ldots\right),\\ v_y &= -\frac{4U\vartheta}{\pi}\sin\varphi\left(1-\tfrac{1}{2}\xi\ln\frac{1+\xi}{1-\xi}-\frac{\cos^2\varphi(2-3\sin^2\varphi)}{12\eta^2}\ \ldots\right). \end{aligned}\right\} \quad \text{(III.21)}$$

For $\eta \to \infty$, these formulæ become identical with (3.9).

It is also easy to examine the induced velocities in the central section (symmetry plane), and in the neighbouring sections. Putting $y = 0$ in (III.14, 15), or $\eta = 0$ in(III.16) we get at once :

$$(v_y)_{y=0} = 0\ ;\ (v_x)_{y=0} = -\frac{4}{\pi}U\vartheta\cos\varphi\left(1-\tfrac{1}{2}\xi\ln\frac{1+\xi}{1-\xi}\,\frac{1+\sin\varphi}{1-\sin\varphi}\right), \quad \ldots \quad \text{(III.22)}$$

(*see* 6.1). For small y, it is seen directly from (III.14) that v_x differs from (III.22) only by small terms of the order y^2, and this shows that the lines $v_x = \text{const.}$ (approximate isobars, *cf.* Fig. 8) cut the x-axis at right angles.

It may be useful to expand the complicated formulæ (III.16, 17, 18) into power series in η, to show the behaviour of the induced velocities near the central section. We get :

$$\left.\begin{aligned} r_1 &= (1+\xi)\cos\varphi - \eta\sin\varphi + \frac{\eta^2}{2(1+\xi)}\cos\varphi + \frac{\eta^3}{2(1+\xi)^2}\sin\varphi\\ &\quad + \frac{\eta^4}{8(1+\xi)^3}\,\frac{4\sin^2\varphi-\cos^2\varphi}{\cos\varphi}\ \ldots,\\ r_2 &= (1-\xi)\cos\varphi + \eta\sin\varphi + \frac{\eta^2}{2(1-\xi)}\cos\varphi - \frac{\eta^3}{2(1-\xi)^2}\sin\varphi\\ &\quad + \frac{\eta^4}{8(1-\xi)^3}\,\frac{4\sin^2\varphi-\cos^2\varphi}{\cos\varphi}\ \ldots, \end{aligned}\right\} \quad \text{(III.23)}$$

$$\left.\begin{aligned} \ln F_1 &= \ln\frac{1+\xi}{1-\xi}\,\frac{1+\sin\varphi}{1-\sin\varphi} - \frac{2\eta}{1-\xi^2}\tan\varphi\\ &\quad + \frac{\eta^2}{(1-\xi^2)^2}\,\frac{\sin\varphi}{\cos^2\varphi}\,(1+\xi^2+4\xi\sin\varphi)\ \ldots,\\ \ln F_2 &= \ln\frac{1+\xi}{1-\xi}\,\frac{1+\sin\varphi}{1-\sin\varphi} - \frac{2\eta}{1-\xi^2}\,\frac{\xi+2\sin\varphi}{\cos\varphi}\ \ldots,\\ \ln F_3 &= \frac{2\eta}{1-\xi^2}\,\frac{\xi+\sin\varphi}{\cos\varphi} - \frac{2\eta^2\sin\varphi}{(1-\xi^2)^2}\,\frac{1+\xi^2+2\xi\sin\varphi}{\cos^2\varphi}\ \ldots,\\ \ln F_4 &= 2\ln\frac{2\sqrt{[1-\xi^2]}}{\eta} + \frac{2\xi\eta}{1-\xi^2}\tan\varphi\ \ldots, \end{aligned}\right\} \quad \text{(III.24)}$$

and hence :

$$\left.\begin{aligned} -\frac{\pi}{4\vartheta}\,\frac{v_x}{U\cos\varphi} &= 1-\tfrac{1}{2}(\xi-\eta\tan\varphi)\ln\frac{1+\xi}{1-\xi}\,\frac{1+\sin\varphi}{1-\sin\varphi} + \frac{\xi\eta\tan\varphi}{1-\xi^2}\\ &\quad - \tfrac{1}{2}\eta^2\,\frac{\sin\varphi}{\cos^2\varphi}\,\frac{3\xi-\xi^3+4\sin\varphi}{(1-\xi^2)^2}\ \ldots,\\ -\frac{\pi}{4\vartheta}\,\frac{v_y}{U\sin\varphi} &= +\frac{\eta}{\cos\varphi}\ln\frac{2\sqrt{[1-\xi^2]}}{\eta}\\ &\quad -\tfrac{1}{2}\eta\tan\varphi\left(\ln\frac{1+\xi}{1-\xi}\,\frac{1+\sin\varphi}{1-\sin\varphi} + \frac{\xi}{\sin\varphi}\,\frac{\xi+\sin\varphi}{1-\xi^2}\right) + \eta^2\,\frac{\sin\varphi}{\cos^2\varphi}\,\frac{3\xi-\xi^3+2\sin\varphi}{(1-\xi^2)^2}\ \ldots \end{aligned}\right\} \quad \text{(III.25)}$$

APPENDIX IV

Velocity Distribution in the Symmetry Plane of Swept-back Wings with Arbitrary Profiles

Let us consider a *kinked source filament* of constant strength Q per unit length in xy-plane, with its vertex at the origin O, and an arbitrary point P (x, z) in the symmetry plane (Fig. 24). It will be required to find the component v_x' of the velocity induced by the filament at P. This component will obviously consist of two equal parts contributed by the two parts of the kinked filament, so let us consider the right hand part $(0, +\infty)$ only. Drawing a plane Π through that part of the filament and the point P, the total velocity v_i induced by that part will lie in Π, and its two components v_1 (parallel to $0, +\infty$) and v_2 (perpendicular to $0, +\infty$) may be found as in Appendix II (formulæ II.7) :

$$v_1 = \frac{Q}{4\pi h}\cos\beta\ ;\quad v_2 = \frac{Q}{4\pi h}\ (1 - \sin\beta), \qquad \text{(IV.1)}$$

there being obvious changes in signs.

The component v_2 may be resolved into two sub-components v_z' and v_n'

$$v_z' = v_2\sin\gamma\ ;\quad v_n' = v_2\cos\gamma, \qquad \text{(IV.2)}$$

where γ is the angle between the planes xy and Π. The two components v_2 and v_n' now lie both in a plane parallel to xy, and hence (Fig. 24a) :

$$\tfrac{1}{2}v_x' = v_n'\cos\varphi + v_1\sin\varphi = \frac{Q}{4\pi h}\left\{(1 - \sin\beta)\cos\gamma\cos\varphi + \cos\beta\sin\varphi\right\}. \qquad \text{(IV.3)}$$

Using the obvious geometric relationships :

$$\left.\begin{aligned} h^2 &= x^2\cos^2\varphi + z^2,\ \cos\gamma = \frac{x\cos\varphi}{h}, \\ \cos\beta &= \frac{h}{\sqrt{(x^2+z^2)}},\ \sin\beta = \frac{x\sin\varphi}{\sqrt{(x^2+z^2)}}, \end{aligned}\right\} \qquad \text{(IV.4)}$$

we finally bring v_x' to the form :

$$v_x' = \frac{Q}{2\pi}\,\frac{x(x^2+z^2)^{1/2}\cos^2\varphi + z^2\sin\varphi}{(x^2+z^2)^{1/2}\,(x^2\cos^2\varphi + z^2)}, \qquad \text{(IV.5)}$$

or, simplifying :

$$v_x' = \frac{Q}{2\pi}\,\frac{x + (x^2+z^2)^{1/2}\sin\varphi}{x^2 + z^2 + x(x^2+z^2)^{1/2}\sin\varphi} \qquad \text{(IV.6)}$$

(*cf.* 7.1). For $z = 0$, we get $v_x' = Q/2\pi x$, whether x is positive or negative, in agreement with the result found earlier in section 4. It is obvious that the velocity distribution in the xz-plane is not symmetrical with respect to the z-axis. This distribution may be examined most conveniently in polar co-ordinates. Putting $x = \varrho\cos\psi$, $z = \varrho\sin\psi$, we get :

$$\frac{2\pi}{Q}v_x' = \frac{1}{\varrho}\,\frac{\cos\psi + \sin\varphi}{1 + \sin\varphi\cos\psi}, \qquad \text{(IV.7)}$$

and hence any locus of $v_x' = \text{const.}$ will be represented by the equation :

$$\varrho = d\,\frac{\cos\psi + \sin\varphi}{1 + \sin\varphi\cos\psi}. \qquad \left[d = \frac{Q}{2\pi v_x'}\right]. \qquad \text{(IV.8)}$$

Reversing the sign of d will also reverse that of v_x'. Two such loci are represented in Fig. 10: and all other loci will be curves similar to the given ones, except the locus $v_x' = 0$ which consists of two semi-infinite straight lines $\varphi = \pm [(\pi/2) + \varphi]$. If $\varphi = 0$, the formula (IV.6) becomes simply:

$$v_x' = \frac{Q}{2\pi} \frac{x}{x^2 + z^2},$$

and the loci $v_x' = \text{const.}$ become circles, the induced velocity field being symmetrical.

It is now possible to deduce a general formula for the velocity distribution in the *central section of a swept-back wing with an arbitrary symmetrical profile,* following a method similar to that used in Appendix I for unswept wings. The strength of an infinitesimal kinked source filament (Fig. 4) will be:

$$Q = q(\bar{x})\, d\bar{x} \cos\varphi = -2U \,.\, F'(\bar{x}) \,.\, d\bar{x} \cos\varphi\,, \quad .. \quad .. \quad .. \quad .. \quad \text{(IV.9)}$$

where $z = F(x)$ is the equation of the profile. The infinitesimal velocity induced by the filament at a point (x, z) is, after (IV.6):

$$dv_x = -\frac{U}{\pi} F'(\bar{x}) \,.\, \cos\varphi \frac{x - \bar{x} + [(x-\bar{x})^2 + z^2]^{1/2} \sin\varphi}{(x-\bar{x})^2 + z^2 + (x-\bar{x})\,[(x-\bar{x})^2 + z^2]^{1/2} \sin\varphi}\, d\bar{x}\,, \quad .. \quad \text{(IV.10)}$$

and we have to integrate this expression from $\bar{x} = -b$ to $\bar{x} = +b$, and let z tend to zero *afterwards.* One example of such an integration has been given in Section 7 for the parabolic profile, and it suggests a method to be used in the general case. It will be convenient to compare the induced velocity on a swept-back wing with that on a straight wing, as given in Appendix I by (I.4). We get:

$$\frac{1}{\cos\varphi} v_x - (v_x)_{\varphi=0}$$

$$= -\frac{U}{\pi} \int_{-b}^{b} \left[\frac{x - \bar{x} + [(x-\bar{x})^2 + z^2]^{1/2} \sin\varphi}{(x-\bar{x})^2 + z^2 + (x-\bar{x})\,[(x-\bar{x})^2 + z^2]^{1/2} \sin\varphi} - \frac{x - \bar{x}}{(x-\bar{x})^2 + z^2} \right] F'(\bar{x})\, d\bar{x}, \quad \text{(IV.11)}$$

which may be brought to:

$$\frac{1}{\cos\varphi} v_x - (v_x)_{\varphi=0} = -\frac{U}{\pi} F'(x)\, I' - \frac{Uz}{\pi} I'', \quad .. \quad .. \quad .. \quad .. \quad .. \quad .. \quad \text{(IV.12)}$$

where:

$$I' = \int_{-b}^{b} \frac{z^2 \sin\varphi\, d\bar{x}}{\{(x-\bar{x})^2 + z^2\}\{\sqrt{[(x-\bar{x})^2 + z^2]} + (x-\bar{x})\sin\varphi\}}$$

$$= \left| \ln\left\{ 1 + \frac{x - \bar{x}}{(x-\bar{x})^2 + z^2} \sin\varphi \right\} \right|_{\bar{x}=b}^{-b}$$

$$= \ln\left\{ 1 + \frac{b + x}{\sqrt{[(b+x)^2 + z^2]}} \sin\varphi \right\} - \ln\left\{ 1 - \frac{b - x}{\sqrt{[(b-x)^2 + z^2]}} \sin\varphi \right\}, \quad \text{(IV.13)}$$

and:

$$I'' = \int_{-b}^{b} \frac{F'(\bar{x}) - F'(x)}{\{(x-\bar{x})^2 + z^2\}\{\sqrt{[(x-\bar{x})^2 + z^2]} + (x-\bar{x})\sin\varphi\}} z \sin\varphi \,.\, d\bar{x}$$

$$= K'' \int_{-b}^{b} \frac{(\bar{x} - x)\, z \sin\varphi\, d\bar{x}}{\{(x-\bar{x})^2 + z^2\}\{\sqrt{[(x-\bar{x})^2 + z^2]} + (x-\bar{x})\sin\varphi\}}, \quad .. \quad \text{(IV.14)}$$

where K'' is a certain mean value of $F''(x)$, smaller than the upper limit of $|F''(x)|$. The integral in (IV.14) can be determined as follows :

$$\frac{I''}{K''} = \left[\frac{1}{\cos\varphi} \cdot \tan^{-1}\left(\frac{\bar{x}-x}{z}\cos\varphi\right) + \frac{1}{\cos\varphi}\tan^{-1}\frac{(\bar{x}-x)^2+z^2}{z\tan\varphi} - \tan^{-1}\frac{\bar{x}-x}{z}\right]_{\bar{x}=-b}^{b}, \quad \ldots \text{(IV.15)}$$

and it is seen to tend to a finite limit when $z \to 0$. The entire second term in (IV.12) is thus small of the second order in ϑ and may be neglected. We then get :

$$\lim\left[v_x \sec\varphi - (v_x)_{\varphi=0}\right]. = -\frac{U}{\pi}F'(x)\lim_{z\to 0} I' = -\frac{U}{\pi}F'(x) \cdot \ln\frac{1+\sin\varphi}{1-\sin\varphi}, \quad \ldots \quad \ldots \text{(IV.16)}$$

and finally :

$$v_x = \left[(v_x)_{\varphi=0} - \frac{U}{\pi}F'(x)\ln\frac{1+\sin\varphi}{1-\sin\varphi}\right]\cos\varphi \cdot \quad \ldots \quad \ldots \quad \ldots \quad \ldots \text{(IV.17)}$$

This surprisingly simple formula gives the velocity in the central section of a swept-back wing with an arbitrary profile, once that of an unswept wing with the same profile has been determined, as shown in Appendix I. The formula (7.4) is obviously a special case of (IV.17).

The above argument again fails generally for sections with rounded edges, although it may work satisfactorily in particular cases, especially if the rounded edge is comparatively sharp. In some cases the method fails for unswept wings, while it works well for swept wings, or vice versa. A few curves showing the velocity distribution at a sweep-back angle $\varphi = 53$ deg 8 min are given in Figs. 15, 16, 18, 20 and 21.

It is seen from the diagrams and from (IV.17) that the maximum supervelocity for a swept wing is always shifted backward when compared with that of a straight wing. The second term in the bracket of (IV.17) always causes the supervelocity to decrease ahead of the maximum thickness, and to increase behind it.

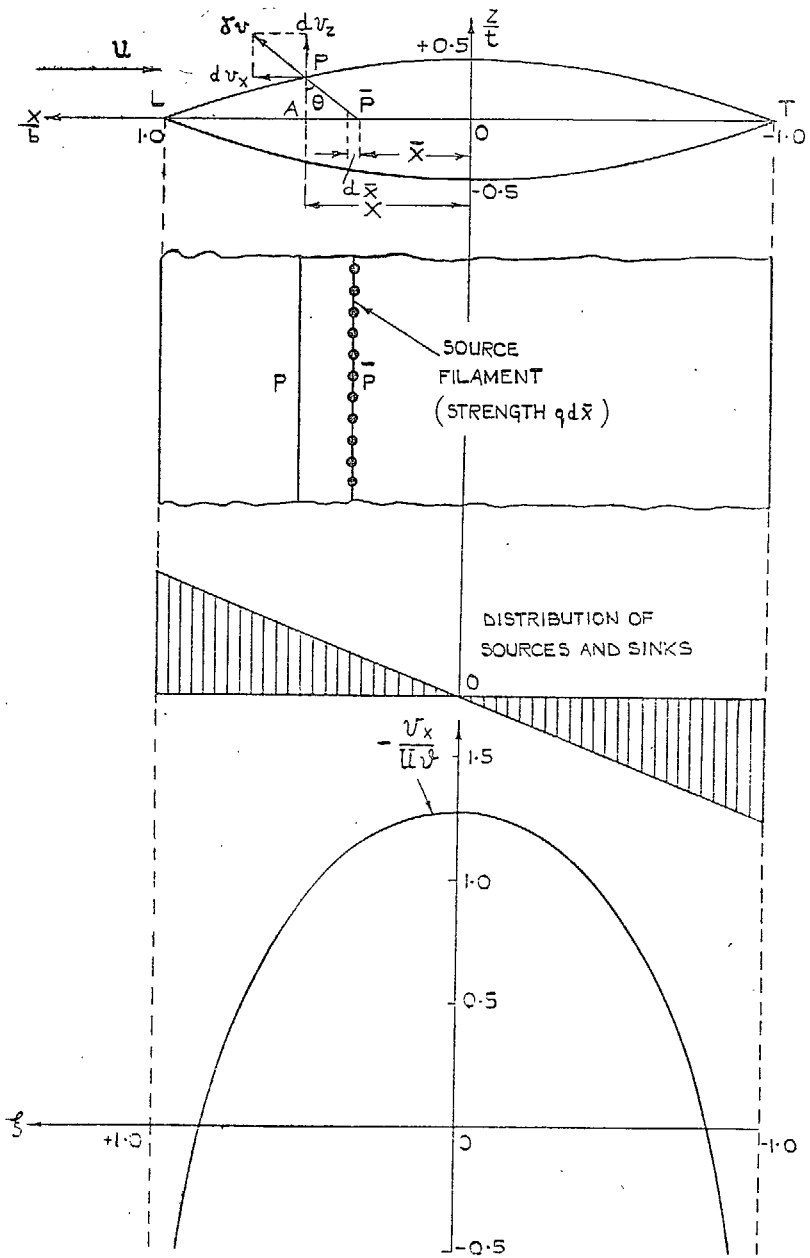

FIG. 1. Distribution of sources and induced velocity for a straight wing with biconvex parabolic profile.

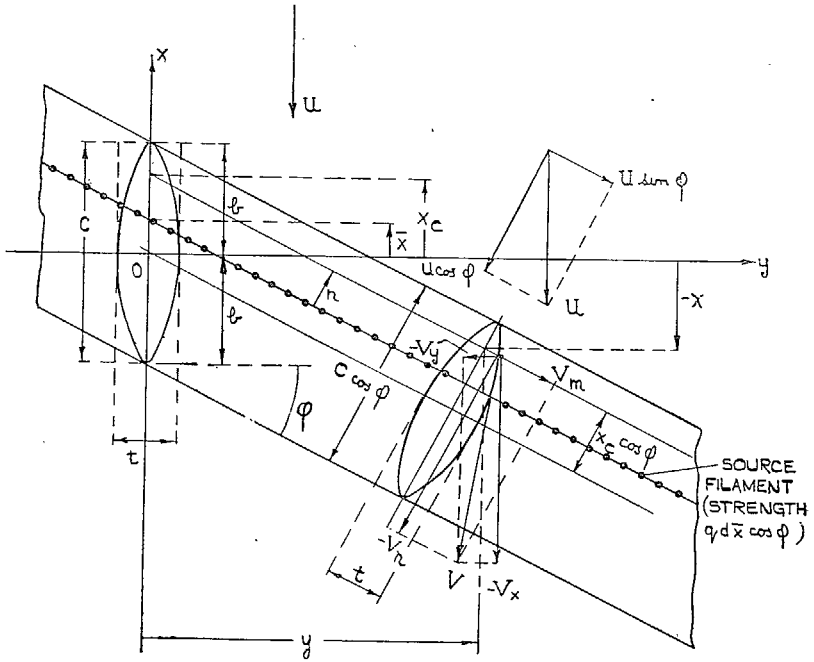

FIG. 2. Sheared wing.

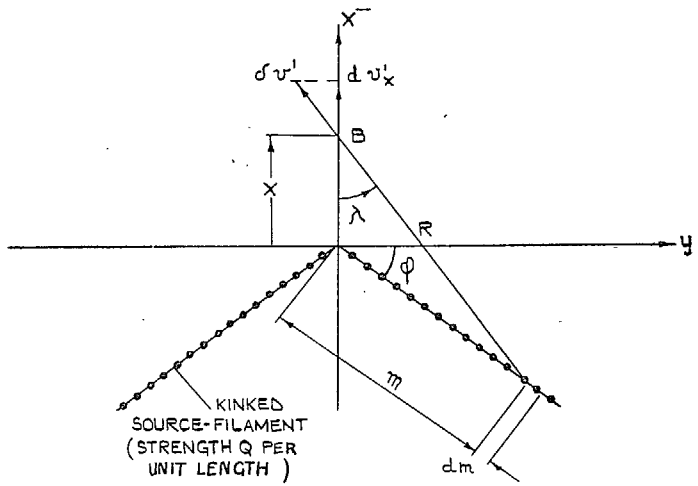

FIG. 3. Velocity induced on x-axis by a kinked source filament in xy-plane.

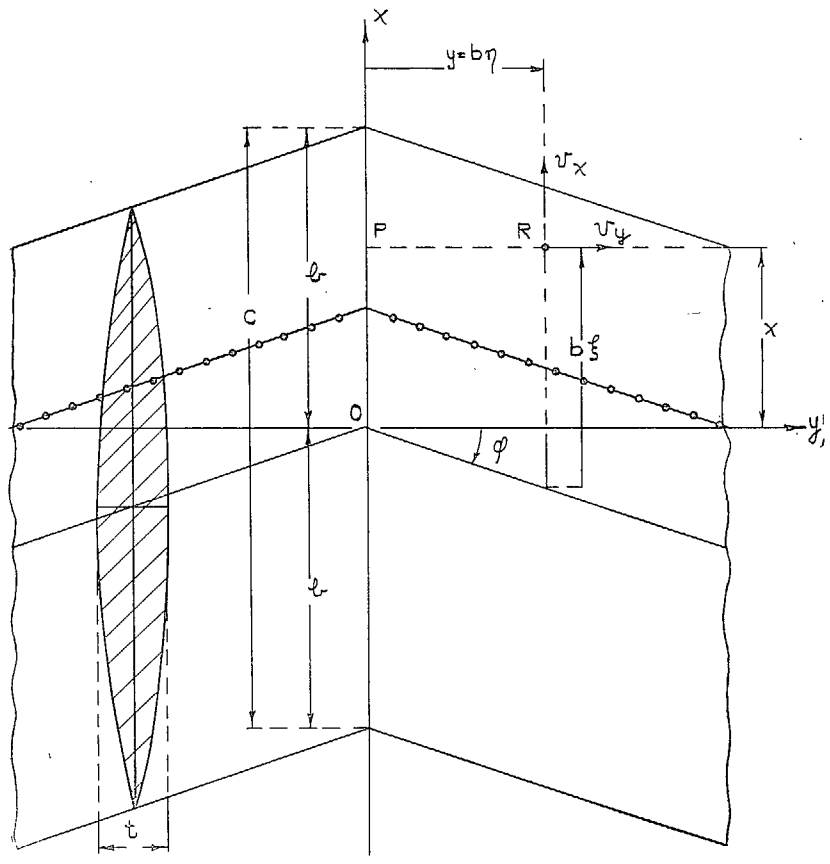

FIG. 4. Infinite swept-back wing.

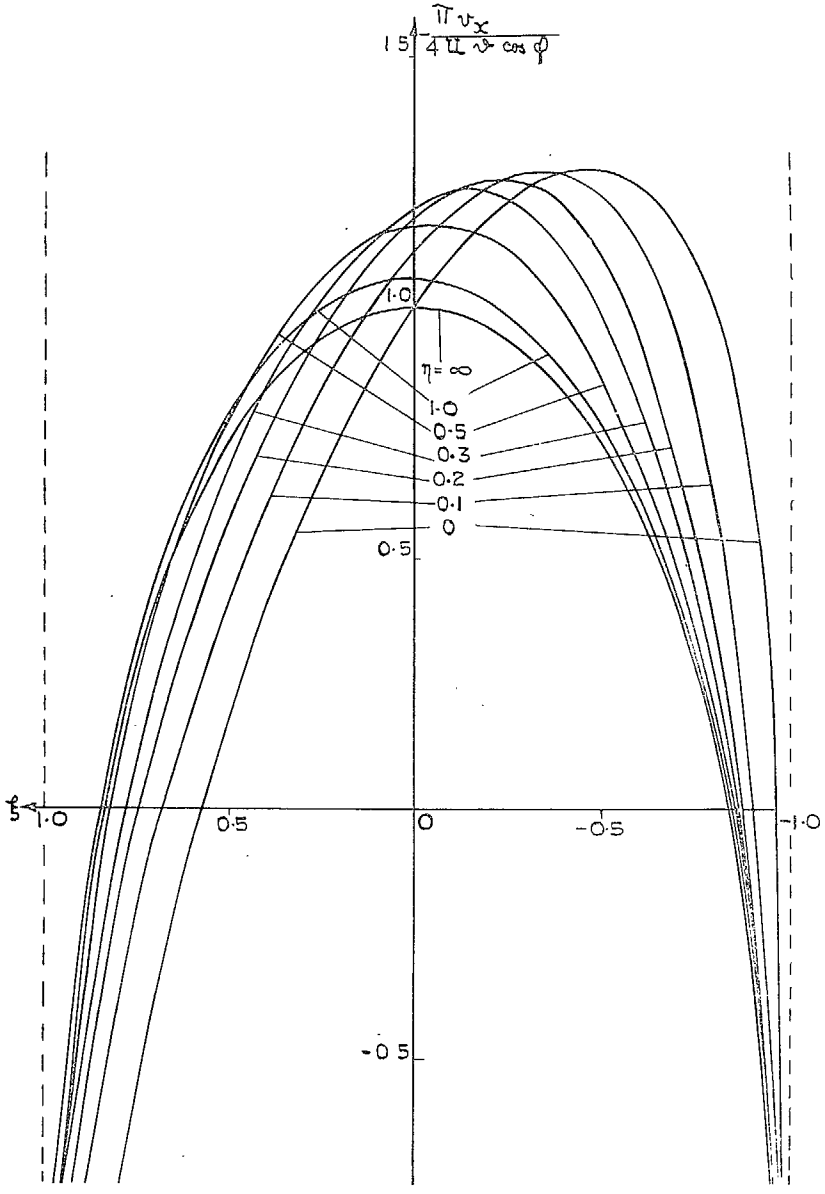

FIG. 5. v_x distribution over a swept-back wing with biconvex parabolic profile.

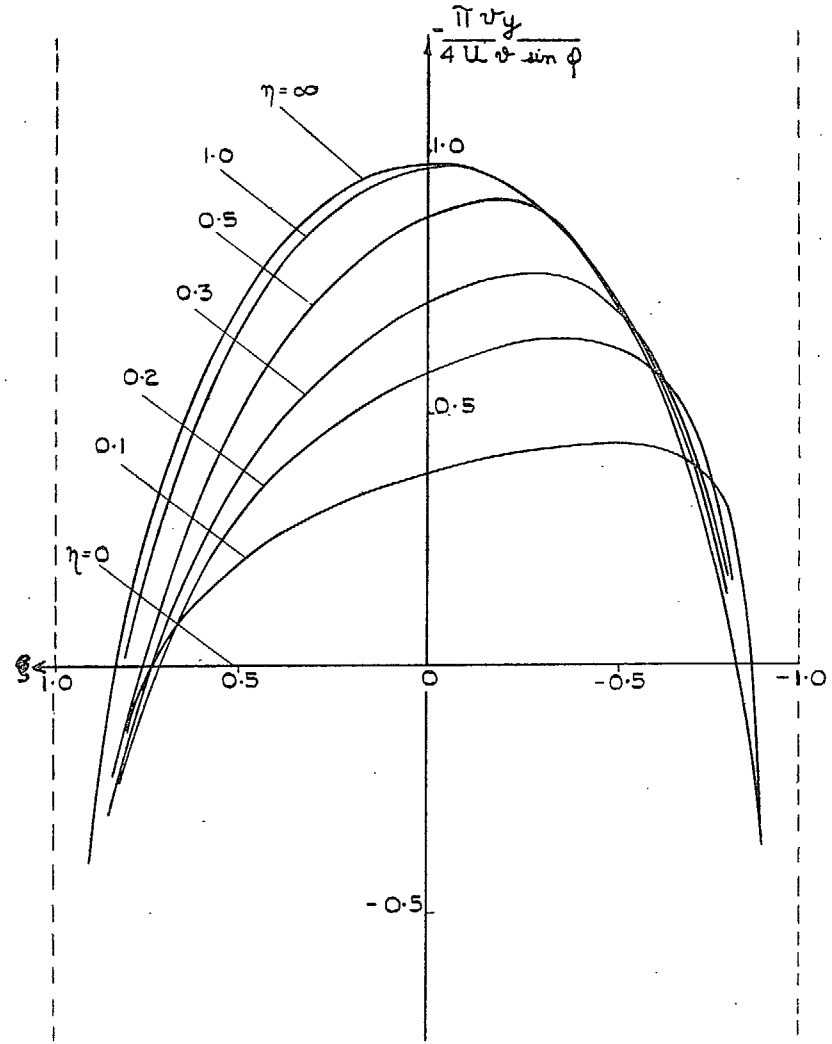

FIG. 6. v_y distribution over a swept-back wing with biconvex parabolic profile.

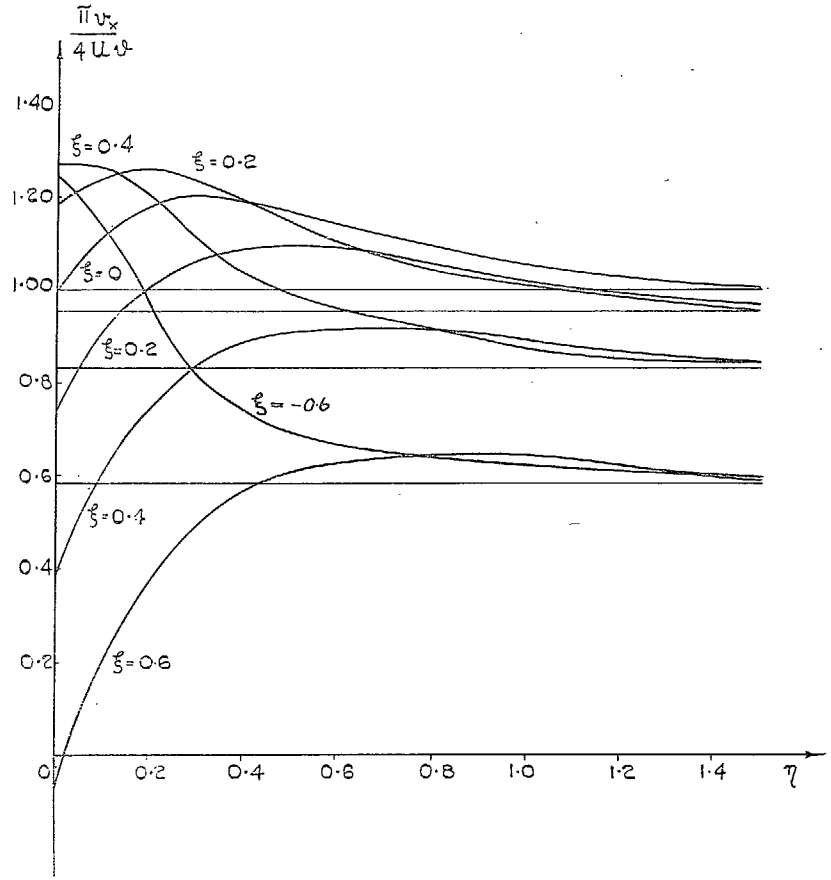

FIG. 7. v_x distribution along lines parallel to wing edges (ξ-parallels).

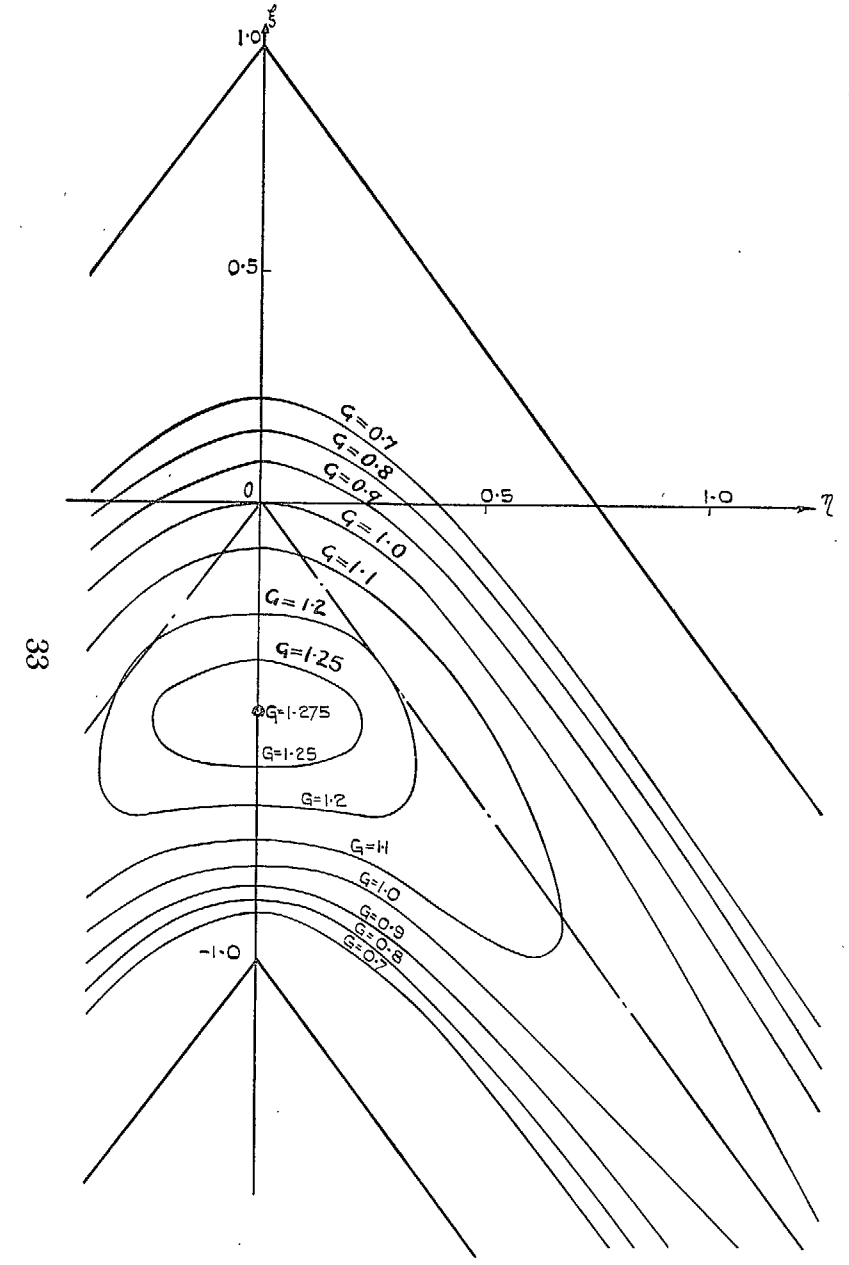

FIG. 8. Isobars on a swept-back wing with biconvex parabolic profile.

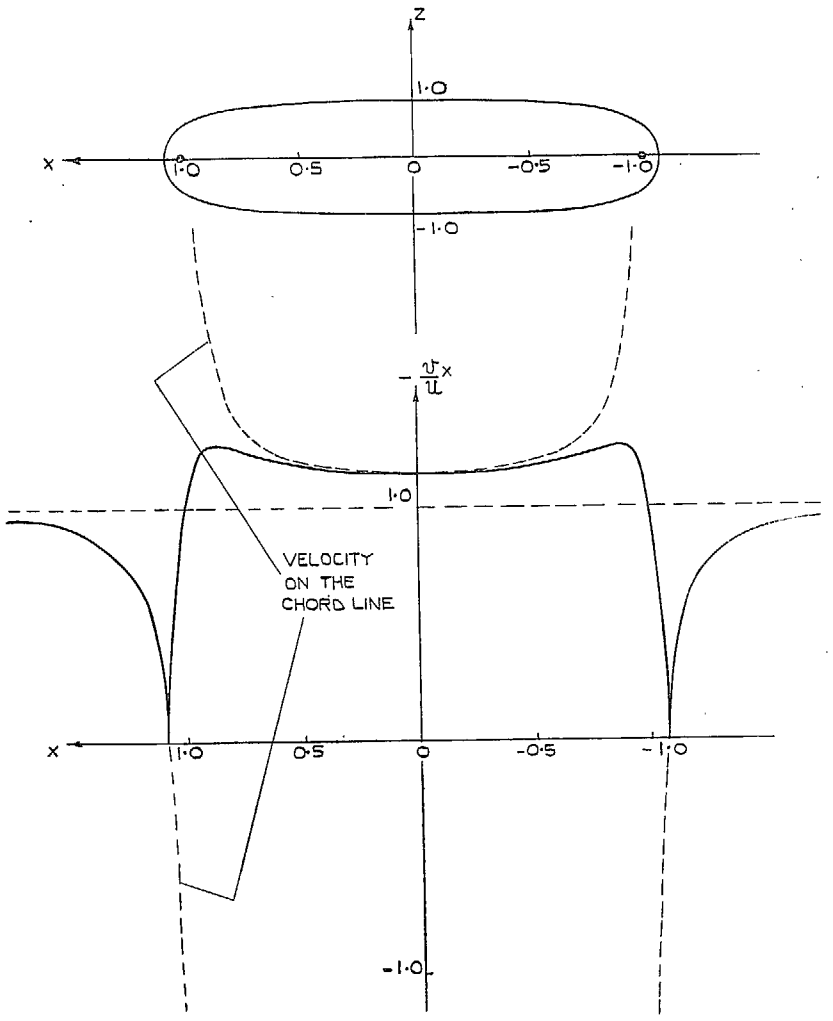

FIG. 9. Velocity distribution on a profile with one source and one sink.

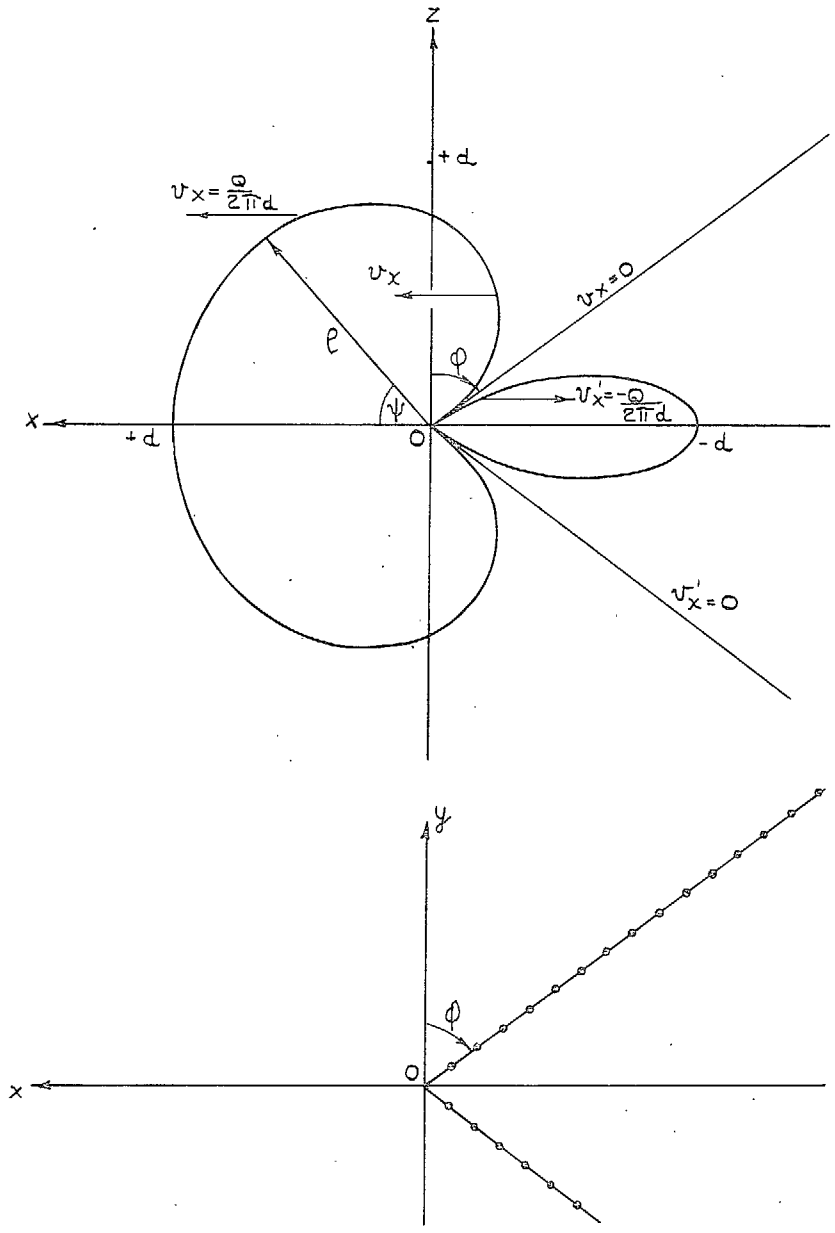

FIG. 10. Loci of constant v_z' in xz-plane induced by a kinked source filament in xy-plane.

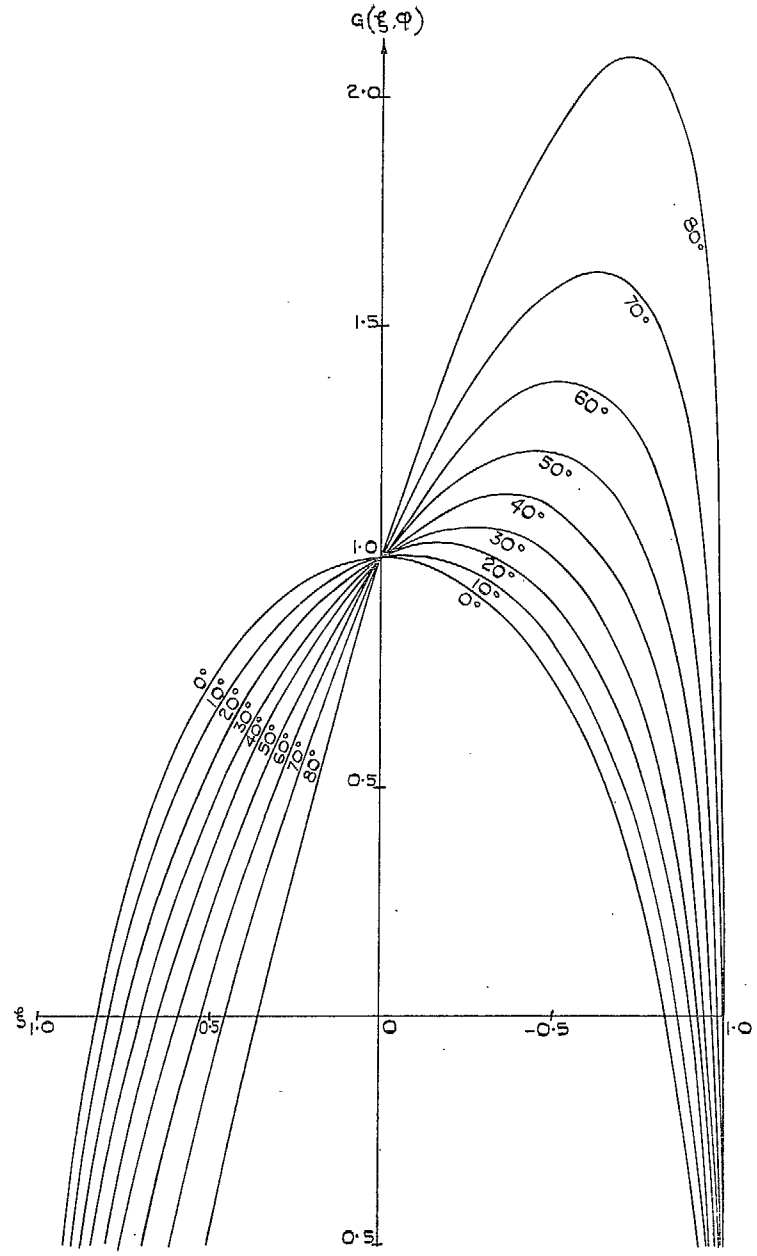

FIG. 11. Graphs of the function $G(\xi, \varphi)$ for different sweep-back angles.

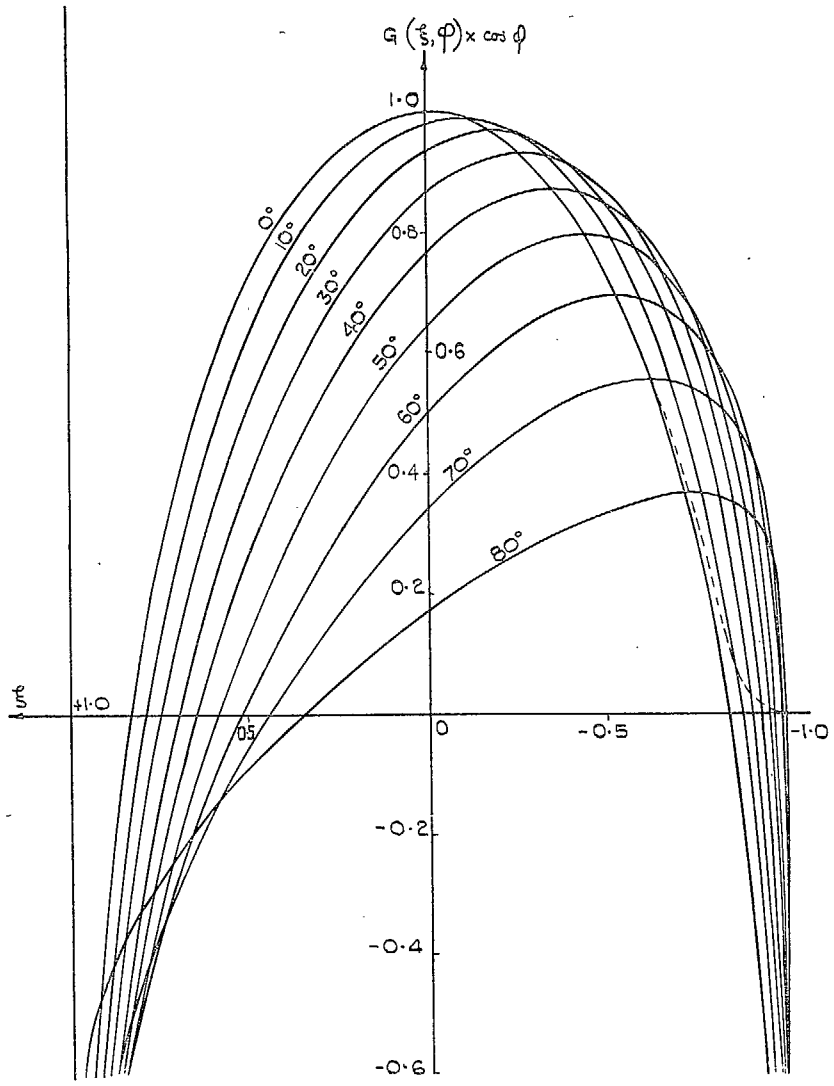

FIG. 12. Graphs of the function $G(\xi,\varphi)\cos\varphi$ for different sweep-back angles.

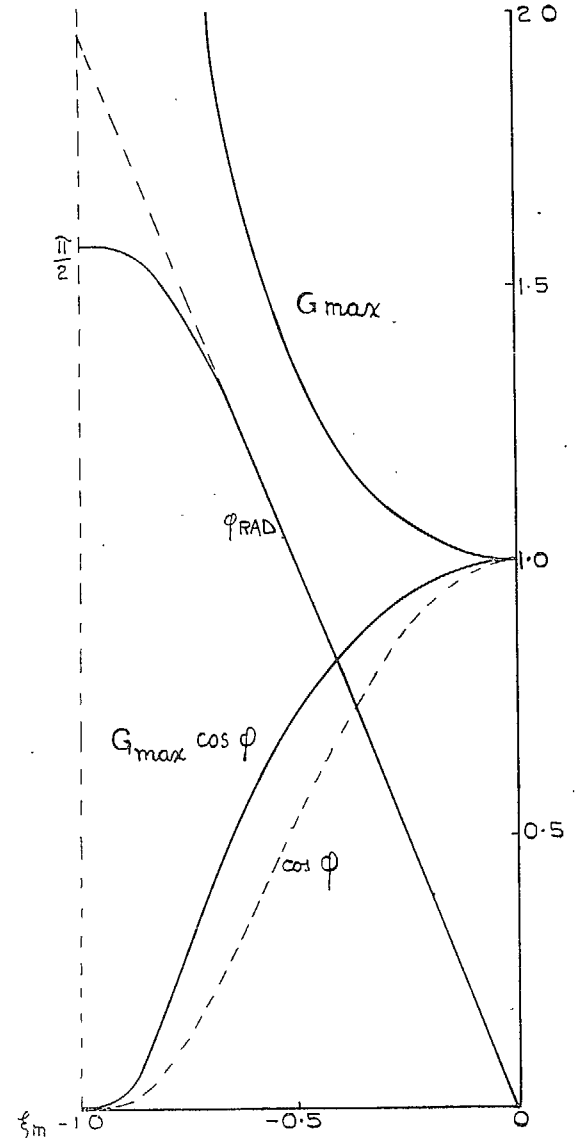

FIG. 13. Maximum supervelocity and its location.

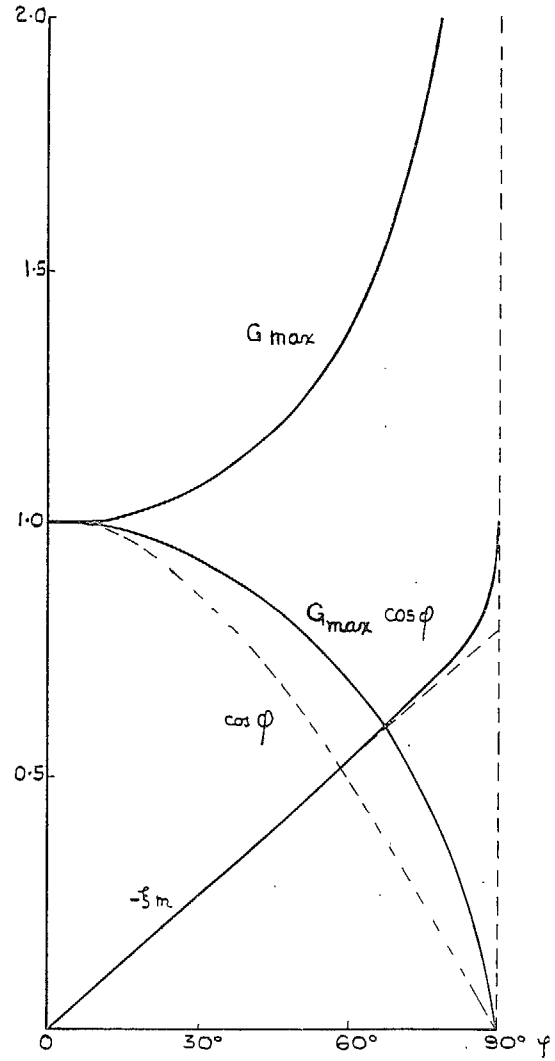

FIG. 14. Maximum supervelocity against angle of sweep-back.

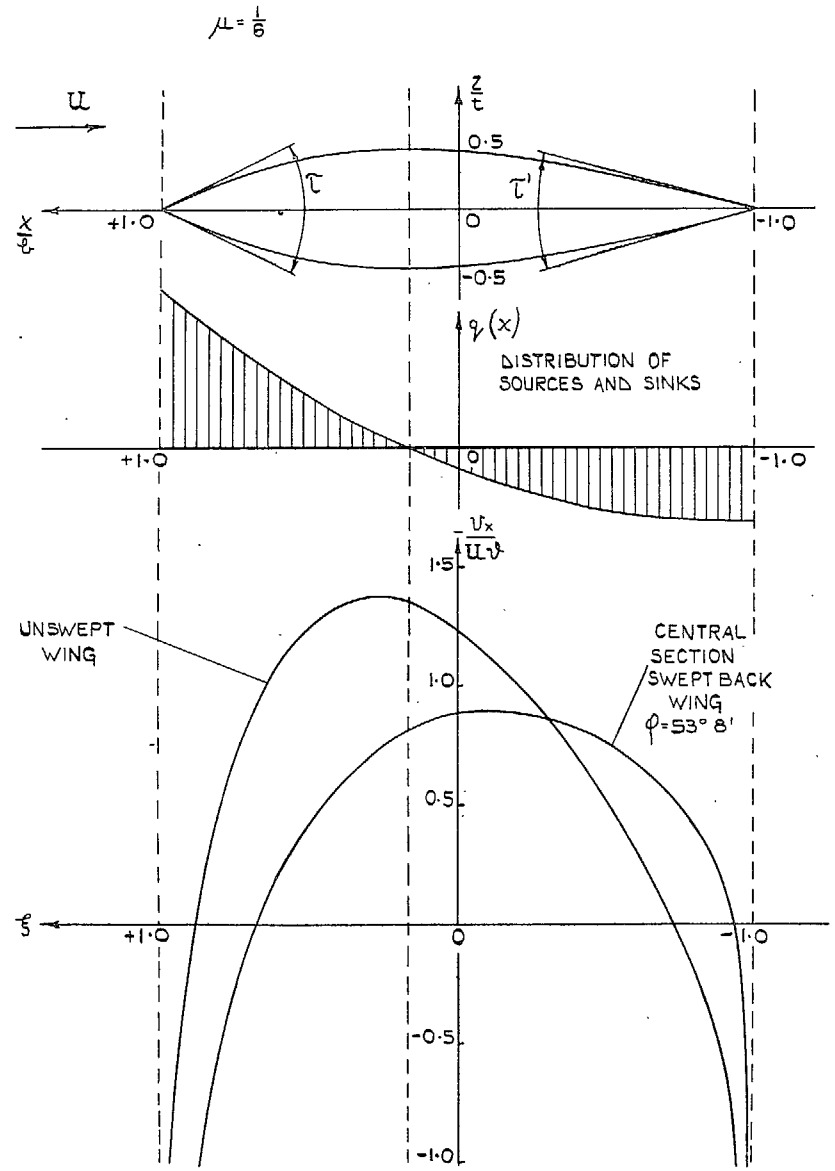

FIG. 15. Profile (I.19) with $\mu = \frac{1}{6}$. Sources and supervelocity distribution.

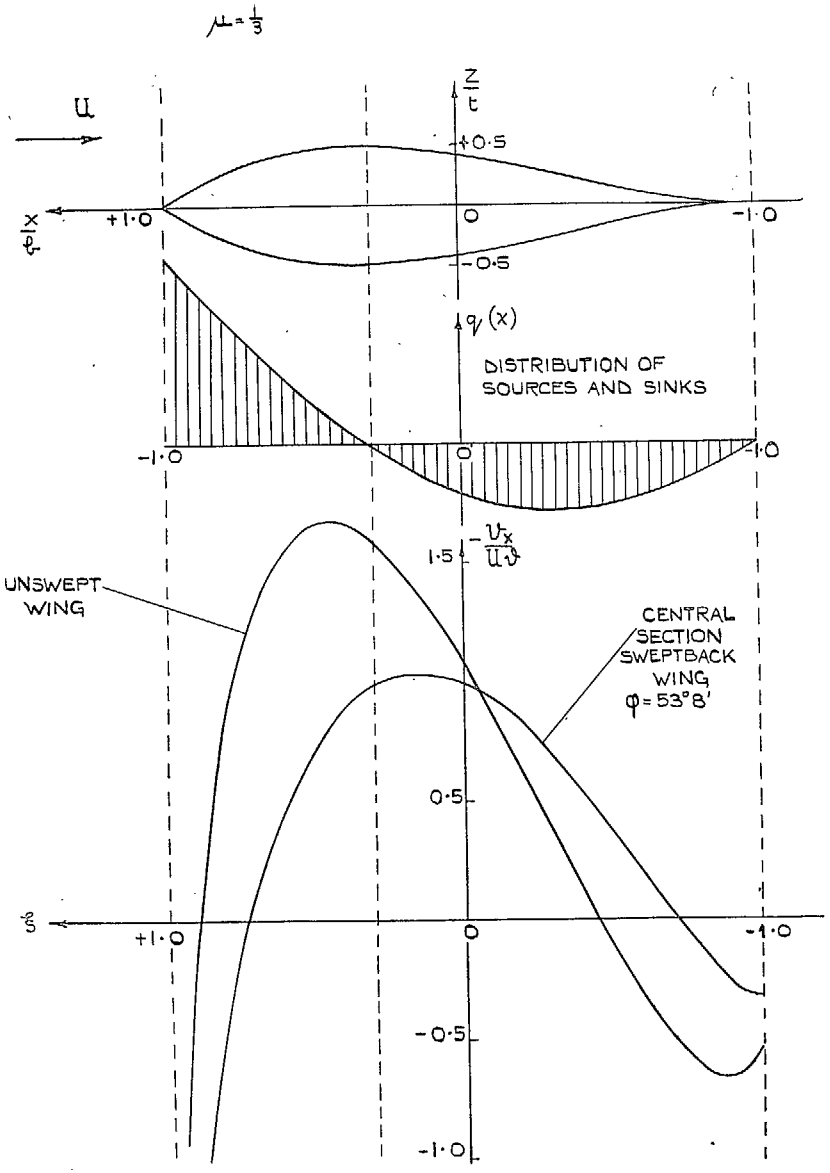

FIG. 16. Profile (I.19) with $\mu = \frac{1}{3}$. Sources and supervelocity distribution.

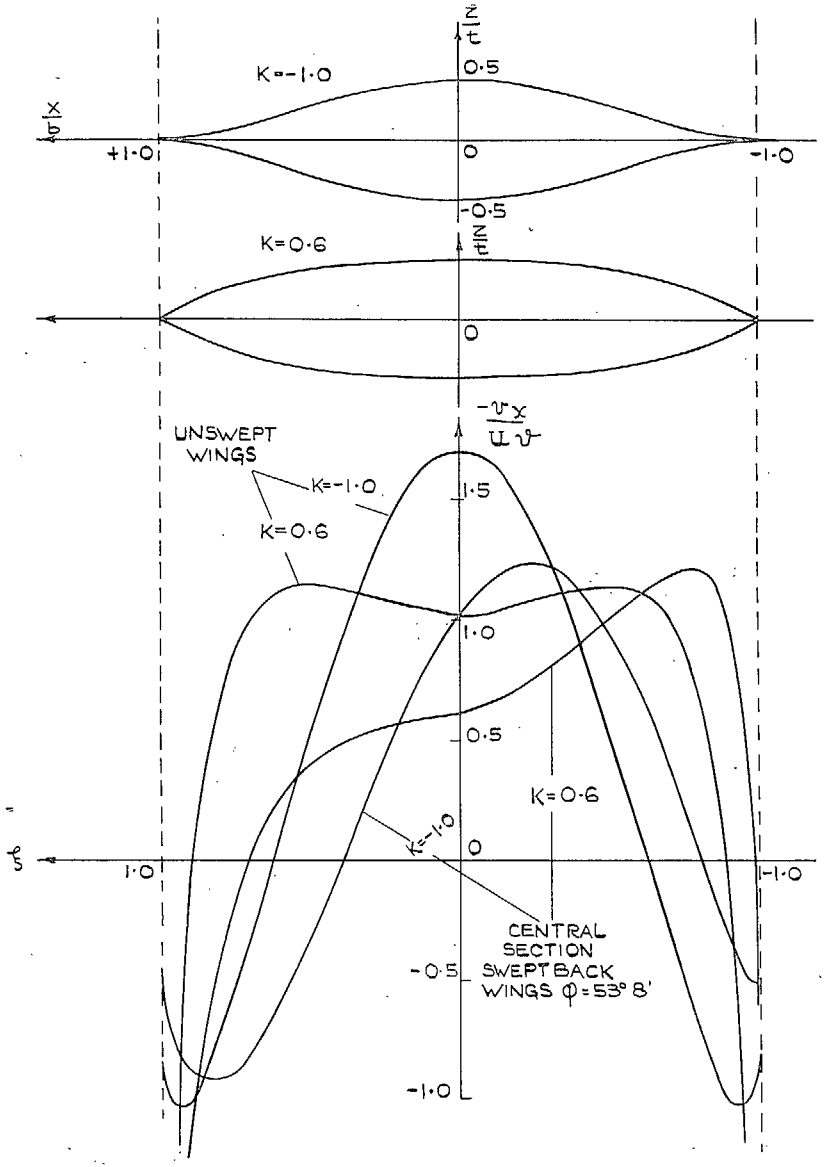

FIG. 17. Profiles (I.23) with $k = 0{\cdot}6$ and $k = -1{\cdot}0$. Supervelocity distribution.

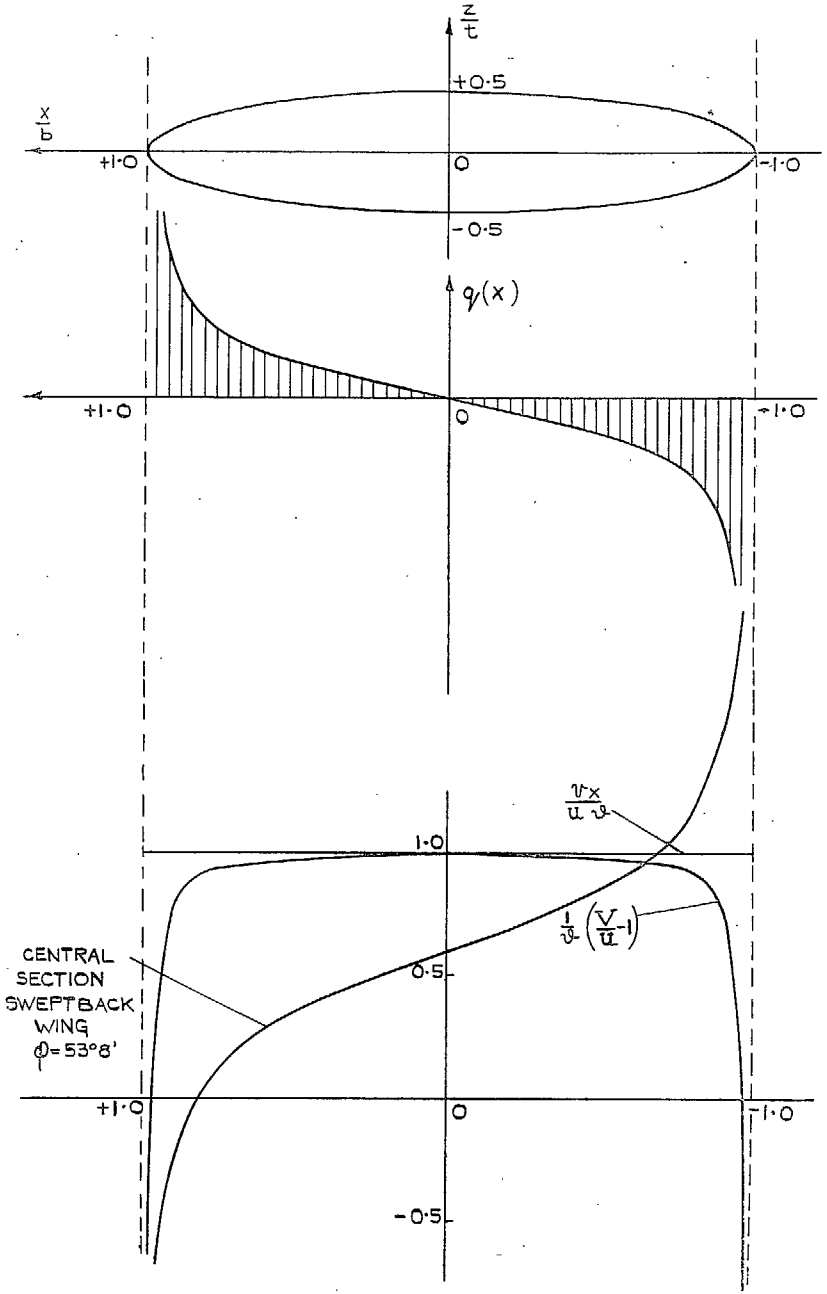

FIG. 18. Elliptic profile. Sources and supervelocity distribution.

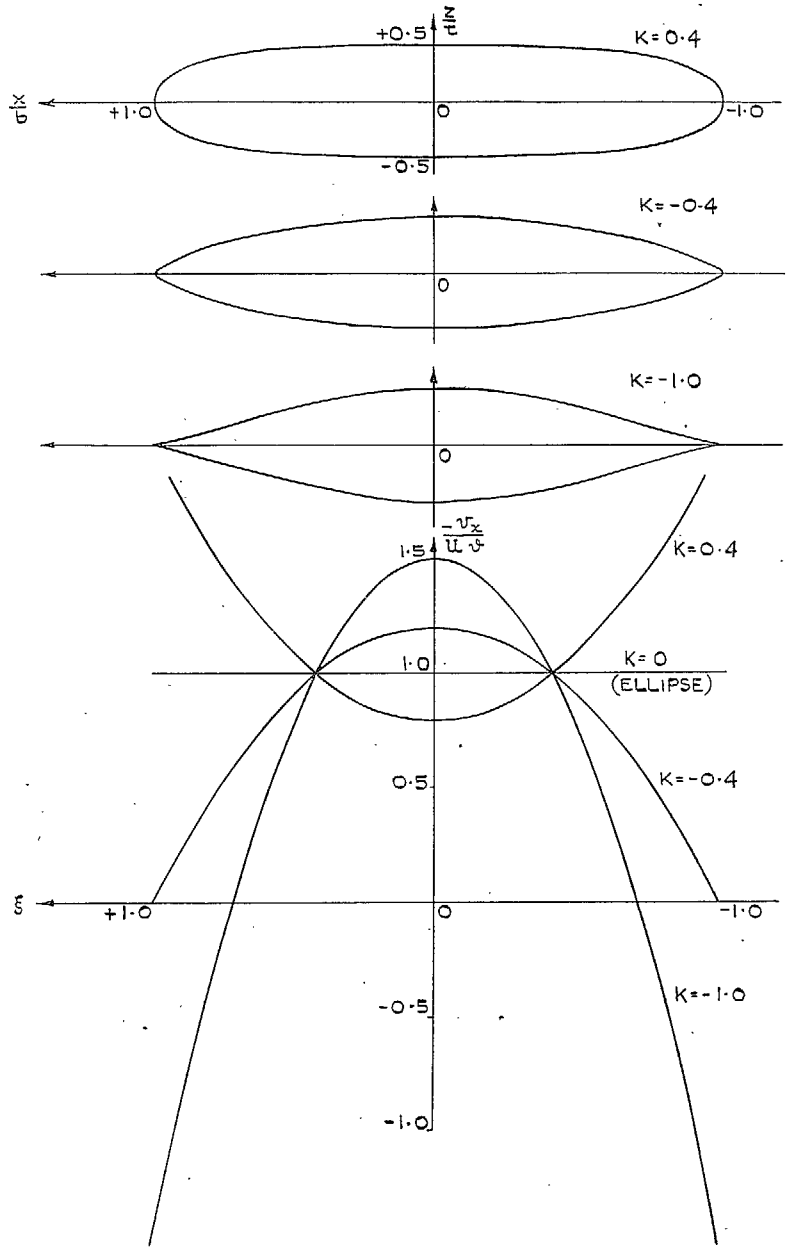

FIG. 19. Profiles (I.41). Supervelocity distribution.

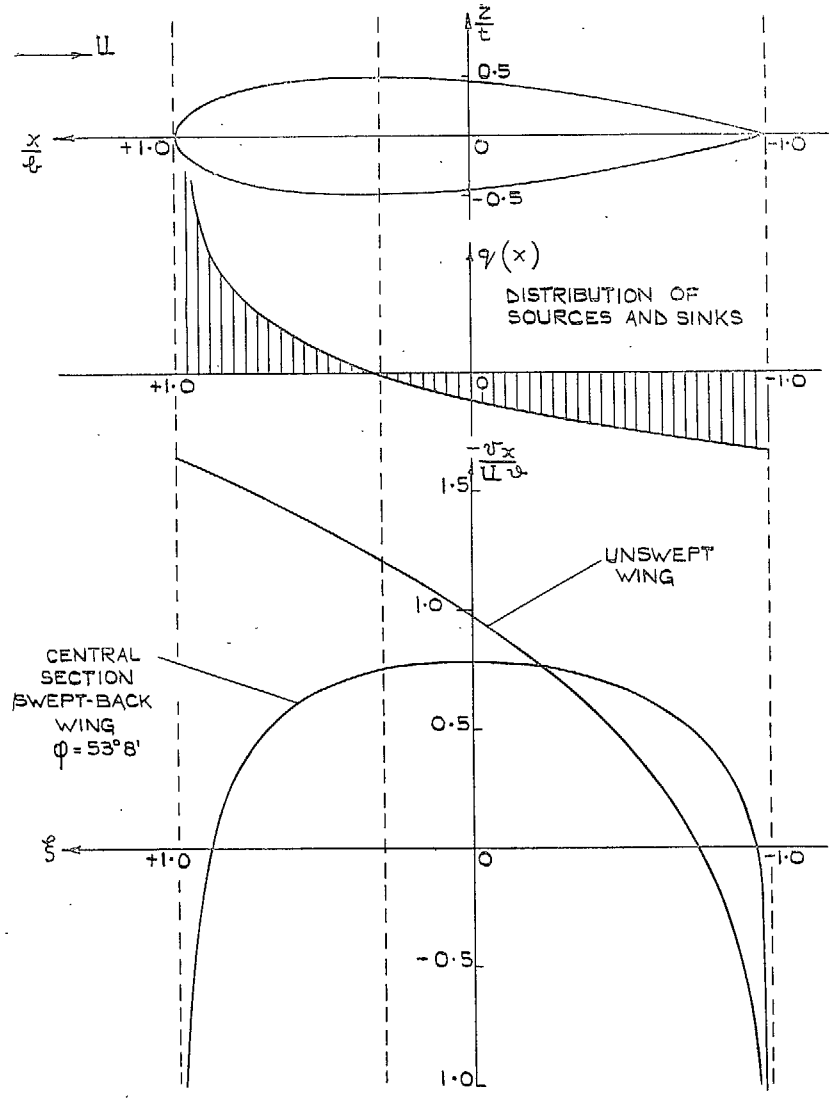

FIG. 20. Profile (I.44). Sources and supervelocity distribution..

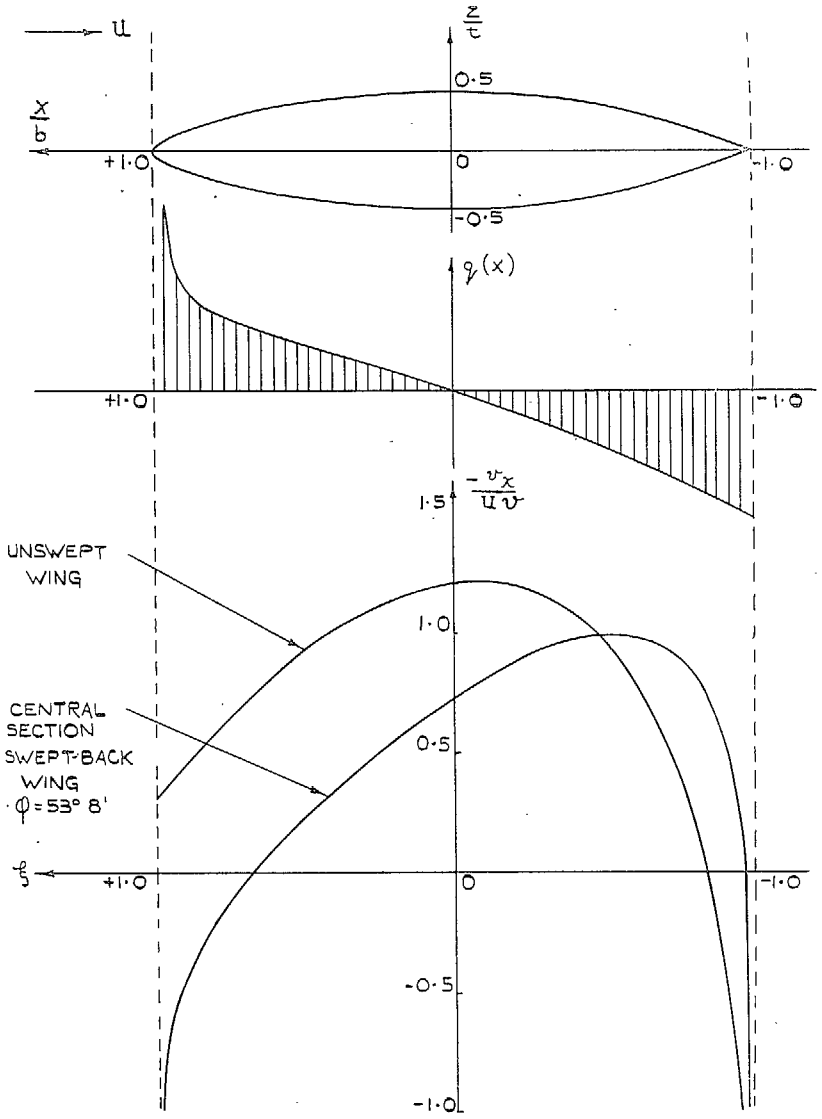

FIG. 21. Profile (I.46). Sources and supervelocity distribution.

J4266 Wt.13/806 K9 D&Co. 10/51 34-263

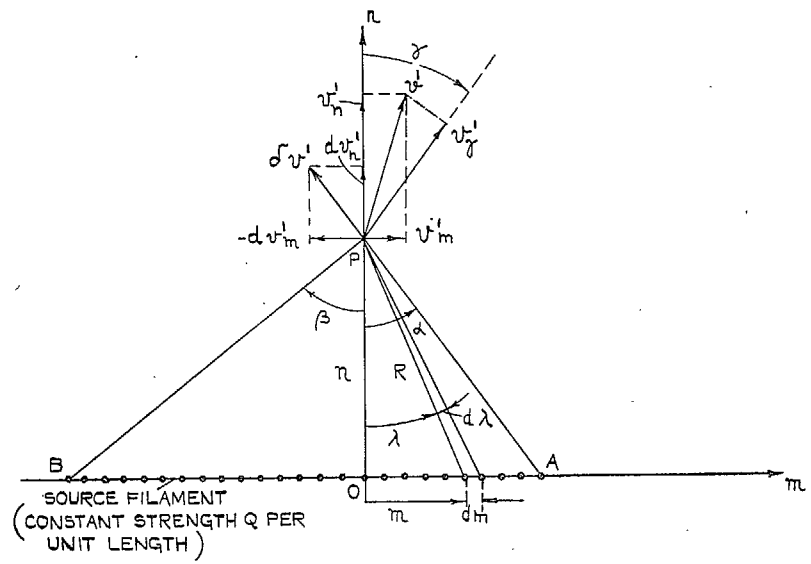

FIG. 22. Velocity induced by a finite source filament.

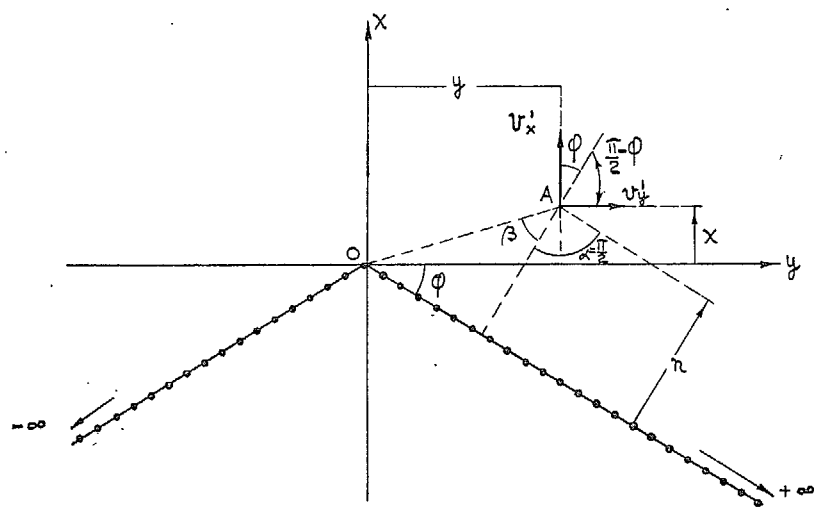

FIG. 23. Velocity induced in *xy*-plane by a kinked source filament in *xy*-plane.

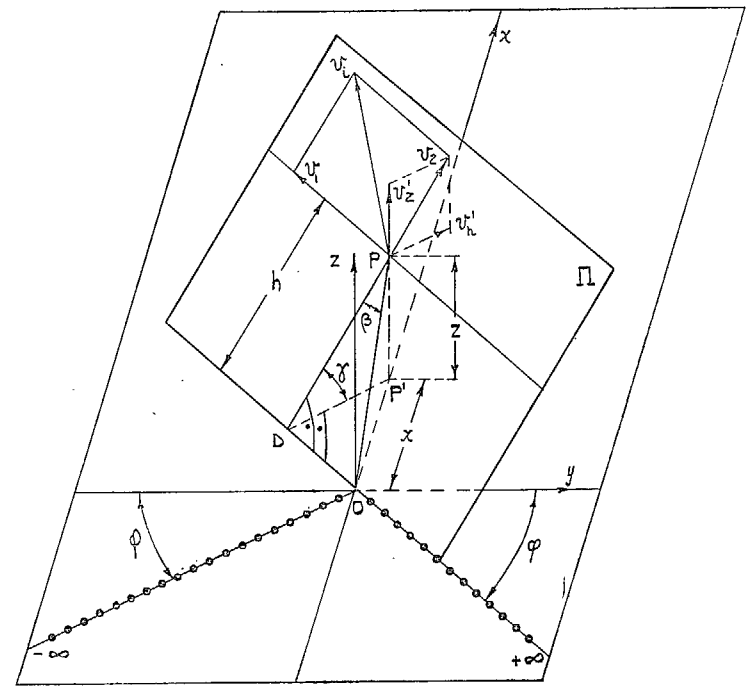

FIG. 24.

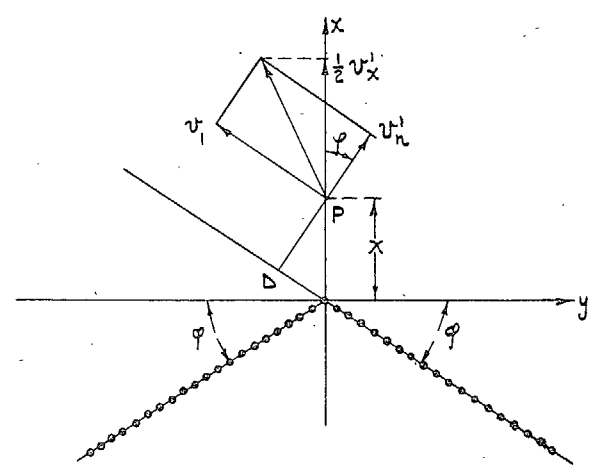

FIG. 24a.

FIGS. 24 and 24a. Velocity induced in *xz*-plane by a kinked source filament in *xy*-plane.

PRINTED IN GREAT BRITAIN

Publications of the Aeronautical Research Council

ANNUAL TECHNICAL REPORTS OF THE AERONAUTICAL RESEARCH COUNCIL (BOUND VOLUMES)—

1934–35 Vol. I. Aerodynamics. *Out of print.*
Vol. II. Seaplanes, Structures, Engines, Materials, etc. 40s. (40s. 8d.)

1935–36 Vol. I. Aerodynamics. 30s. (30s. 7d.)
Vol. II. Structures, Flutter, Engines, Seaplanes, etc. 30s. (30s. 7d.)

1936 Vol. I. Aerodynamics General, Performance, Airscrews, Flutter and Spinning. 40s. (40s. 9d.)
Vol. II. Stability and Control, Structures, Seaplanes, Engines, etc. 50s. (50s. 10d.)

1937 Vol. I. Aerodynamics General, Performance, Airscrews, Flutter and Spinning. 40s. (40s. 10d.)
Vol. II. Stability and Control, Structures, Seaplanes, Engines, etc. 60s. (61s.)

1938 Vol. I. Aerodynamics General, Performance, Airscrews. 50s. (51s.)
Vol. II. Stability and Control, Flutter, Structures, Seaplanes, Wind Tunnels, Materials. 30s. (30s. 9d.)

1939 Vol. I. Aerodynamics General, Performance, Airscrews, Engines. 50s. (50s. 11d.)
Vol. II. Stability and Control, Flutter and Vibration, Instruments, Structures, Seaplanes, etc. 63s. (64s. 2d.)

1940 Aero and Hydrodynamics, Aerofoils, Airscrews, Engines, Flutter, Icing, Stability and Control, Structures, and a miscellaneous section. 50s. (51s.)

Certain other reports proper to the 1940 volume will subsequently be included in a separate volume.

ANNUAL REPORTS OF THE AERONAUTICAL RESEARCH COUNCIL—

1933–34	1s. 6d. (1s. 8d.)
1934–35	1s. 6d. (1s. 8d.)
April 1, 1935 to December 31, 1936.	4s. (4s. 4d.)
1937	2s. (2s. 2d.)
1938	1s. 6d. (1s. 8d.)
1939–48	3s. (3s. 2d.)

INDEX TO ALL REPORTS AND MEMORANDA PUBLISHED IN THE ANNUAL TECHNICAL REPORTS, AND SEPARATELY—

April, 1950 — R. & M. No. 2600. 2s. 6d. (2s. 7½d.)

INDEXES TO THE TECHNICAL REPORTS OF THE AERONAUTICAL RESEARCH COUNCIL—

December 1, 1936 — June 30, 1939.	R. & M. No. 1850.	1s. 3d. (1s. 4½d.)
July 1, 1939 — June 30, 1945.	R. & M. No. 1950.	1s. (1s. 1½d.)
July 1, 1945 — June 30, 1946.	R. & M. No. 2050.	1s. (1s. 1½d.)
July 1, 1946 — December 31, 1946.	R. & M. No. 2150.	1s. 3d. (1s. 4½d.)
January 1, 1947 — June 30, 1947.	R. & M. No. 2250.	1s. 3d. (1s. 4½d.)

Prices in brackets include postage.

Obtainable from

HER MAJESTY'S STATIONERY OFFICE

York House, Kingsway, LONDON, W.C.2 — 423 Oxford Street, LONDON, W.1
P.O. Box 569, LONDON, S.E.1
13a Castle Street, EDINBURGH, 2 — 1 St. Andrew's Crescent, CARDIFF
39 King Street, MANCHESTER, 2 — Tower Lane, BRISTOL 1
2 Edmund Street, BIRMINGHAM, 3 — 80 Chichester Street, BELFAST

or through any bookseller.